A molecular dynamics study on interfacial thermal conductivity between epoxy polymer and alumina fillers in heat-dissipation composite material

(放熱材料内のエポキシ樹脂とアルミナフィラ間の界面熱伝導に関する分子動力学による研究)

by

Kouichi Tanaka

Submitted to

the Department of Scientific and Engineering Simulation

in partial fulfillment of the requirements for the degree of

Doctor of Engineering

at

Nagoya Institute of Technology

2015

Abstract

Heat dissipation materials are essential for automobiles because the temperatures of their electronic components must be kept below certain levels. Such electronic component has been essential particularly for the electric and plug-in hybrid automobiles. For automobiles, a growing trend exists toward high-density packaging of the electronic components and intense use of power IC's. Improvement of the heat dissipation material is highly desired. The heat dissipation material is composed of soft polymer resin and hard filler-particles (called fillers). The fillers, which are about 1−10 micrometer in size, are made of a material with a high thermal conductivity as alumina than the polymers.

Automobile-parts companies have been putting great effort to design a novel heat-dissipation material with a few times higher thermal conductivity than the current ones. However, the enhancement factors of the thermal conductivity of the composite were behind the expectation due to low interfacial thermal conductance between the filler and polymers. The interface in the polymer-ceramic composite is characterized as the system of soft polymer and hard crystalline sub-systems. The phonons in a sub-system are scattered partly at the interface. Such phonon scattering events create a temperature gap at the interface, which relates to the interfacial thermal conductance. A candidate technique to increase the interfacial thermal conductance is coating the fillers by the surface coupling (SC) agent, which is made of organic molecules and acts to connect the fillers and polymers tightly. It was demonstrated experimentally that addition of the SC agent, increases the effective thermal conductivity significantly. Theoretical understanding of its mechanisms is highly desired to clarify the theoretical upper limit and to design a better SC agent for the composite material.

The non-equilibrium molecular dynamics (NEMD) simulation with a

realistic setting is best suited to address the issue of interfacial thermal conductance in the polymer-ceramic composite. In this thesis, We investigate the effects of the SC molecules on the interfacial thermal conductance.

The bisphenol-A (bisA) epoxy molecules are considered for the polymers, α-alumina for the filler, and a model molecule for the SC. The inter-atomic potential between the α-alumina and SC molecule, which is essential in the present simulation, is constructed to reproduce the calculated energies with the electronic density-functional theory.

We firstly consider the situation of a small packing fraction of fillers. We perform the NEMD simulation to obtain interfacial thermal conductance. We find that the interfacial thermal conductance increases significantly by increasing either number or lengths of the SC molecules. Detailed analyses about the atomic configurations and local temperatures around the interface are performed to identify heat-transfer routes through the interface.

We secondary consider the situation of a high packing fraction of fillers with/without the SC molecules. We perform a series of the NEMD runs by changing the polymer depth and adding the SC molecules to understand their effects on the interfacial thermal conductance. We find that for the interfacial thermal conductance is decreased by decreasing the polymer depth toward the chain length of a single bisA molecule. However, addition of the SC molecules reduces deterioration of thermal conductance of the polymer sub-system for smaller polymer depth.

Finally we explain microscopic mechanisms of SC molecules effect through combined analyses of the atomic vibration spectra of the polymer sub-system and phonon wave-packet dynamics simulation. We find that enhancement of the following three quantities by addition of the SC molecules: the phonon population of the bisA molecules at those frequencies corresponding to that of acoustic phonons of α-alumina, the phonon transmission coefficient from the α-alumina slab to the polymer sub-system for the transverse acoustic phonon, and the group velocity of the transverse acoustic phonon in the polymer sub-system.

Contents

List of Tables

List of Figures

Chapter 1

Introduction

1.1 Motivation

The usage proportion of electronics in an automobile continues to increase. The electronics were installed originally to control engines. Thereafter the electronics have been utilized also to control various systems of automobiles such as the transmission, chassis, and active safety and information systems. In addition to the requirements to control basic systems for running, turning and stopping of automobiles, the requirements relating to safety and comfort have emerged recently for the electronics. To deal with such continuing increases in the number and size of the electronics, the integrated circuit (IC)-utilized modular packaging of them has been used widely in recent automobiles [1,2]. It is beneficial to automobiles not only for their compactness and less weight but also for reliability and functionality.

Environmental issues such as the shortage of energy resources, global warming, and air pollution, have become crucial today. Under the situation automakers have accelerated the development and practical applications of green vehicles or environmentally friendly vehicles, e.g., electric and hybrid automobiles. Essential components of these types of automobiles include motors, invertors, and batteries. As for the inverter that works to convert DC to AC and elevate voltage, the so-called power IC in modular packaging is the core component. The silicon carbide (SiC) based power IC instead of the

Si-based one will be put to practical usage to meet the need of high voltage. Relating to that, further improvement of modular packaging is required also. One of the important techniques that should be realized in the packaging is efficient dissipation of intense heat generated both in time and space in the power IC [1-3].

Figure 1.1 (left) shows a schematic view of heat-dissipation from the power IC. To realize efficient heat dissipation, it is important that heat-transfer from the power IC to a heat sink through a heat dissipation material. Figure 1.1 (right) shows a schematic view of the heat dissipation material. The heat dissipation material for that purpose in the forms of adhesive and bulking agent needs be soft to cover an IC without gaps. Composite systems of soft polymers and hard filler-particles (called fillers) are often used for such heat-dissipation materials [2,4,5]. The fillers, which are about $1-10$ micrometer in size, are made of the materials with higher thermal conductivities than the polymers for enhanced effective thermal conductivity of the heat-dissipation material. A α-alumina, which has nearly 100 times of the thermal conductivity of polymers, is commonly used for the filler.

For its application to IC's the heat-dissipation material should be electrically insulating [6]. Automobile-parts companies have been putting great effort to design a novel heat-dissipation material with a few times higher thermal conductivity than the current ones under the conditions that it is electrically insulating, durable, and low cost.

Various experimental trials were performed to further increase the thermal conductivity of such a polymer-ceramic composite: increasing the packing fraction of fillers and using a material with a higher thermal conductivity as boron nitride for the fillers [7-10]. However, the enhancement factors of the thermal conductivity of the composite were behind the expectation due to low interfacial thermal conductance between the filler and polymers. Reducing the thermal resistance at the interface is the key.
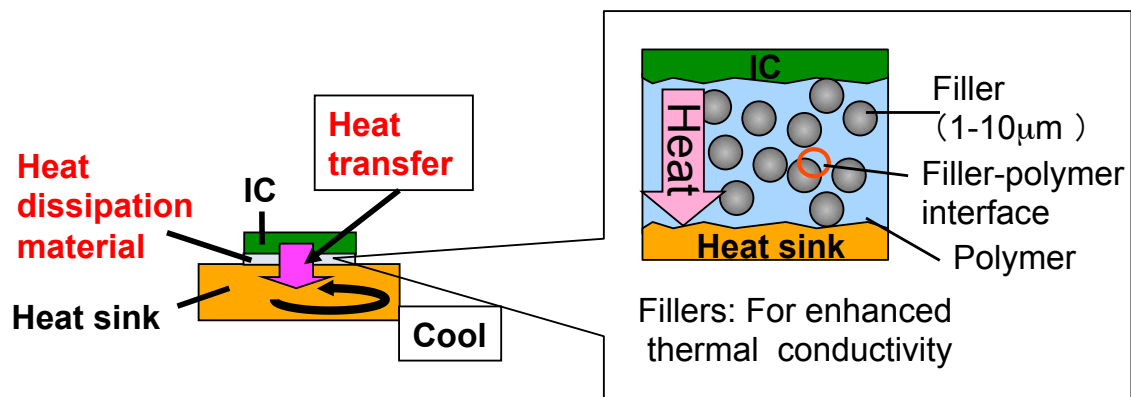
Figure 1.1: Schematic views of (left) heat-dissipation from the power-IC and (right) the heat dissipation material.

The interface in the polymer-ceramic composite is characterized as the system of soft polymer and hard crystalline sub-systems. The phonons in a sub-system are scattered partly at the interface not only by the differences in stiffness and mass density but also by the randomness and reconstructed structures. Such phonon scattering events create a temperature gap at the interface, which relates to the interfacial thermal conductance [11-13].

A candidate technique to increase the interfacial thermal conductance is coating the fillers by the surface coupling (SC) agent, which is made of organic molecules and acts to connect the fillers and polymers tightly as shown Figure 1.2. It was demonstrated experimentally that addition of the silane coupling agent, in fact, increases the effective thermal conductivity significantly at a high packing fraction of the α-alumina fillers [9,10]. Theoretical understanding of its mechanisms is highly desired to clarify the theoretical upper limit and to design a better SC agent for the composite material.
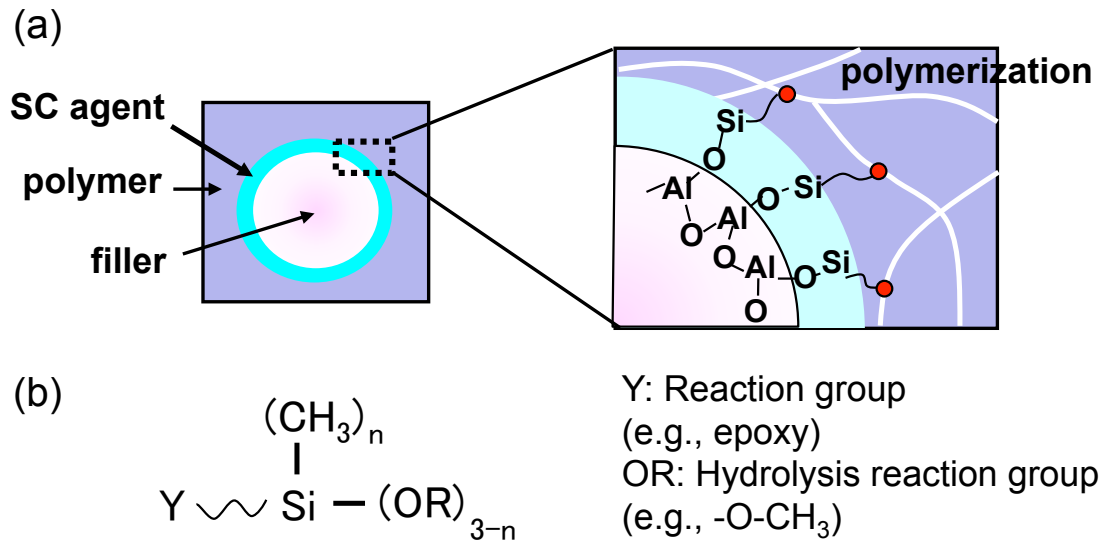
Figure 1.2: (a) Schematic view of a Surface Coupling agents. The SC agents connect filler and polymer tightly. (b) A chemical structure of silan coupling agent.

Sophisticated analytical theories exist to predict the interfacial thermal conductance of ideal interface of two homogeneous sub-systems [14-18]. However, their application to the polymer-ceramic composite is difficult because the polymer sub-system is essentially an entangled chains and hence neither homogeneous nor isotropic at microscopic scales.

Theoretical approach with the classical molecular dynamics (MD) simulation has potential capability to address the issue of understanding the thermal conductivity at microscopic scales. There are two approaches for predicting phonon thermal conductivity through MD simulation. One is the Green-Kubo(GK) method [19,20] and the other is the non-equilibrium method [20-23]. The Green-Kubo method is an equilibrium technique based on the fluctuation-dissipation theorem. Cubic simulation cells with periodic boundary conditions are commonly used. Interpreting the results of the GK method can be challenging for systems with complex unit cells, such as the interface in polymer-ceramic composite. The non-equilibrium MD (NEMD) with a realistic setting is best suited to address the issue of interfacial thermal conductance in the polymer composite [24-29]. In the NEMD, a heat flux is applied to a simulation cell along the direction of interest. Using the

imposed heat flux and the resulting steady-state temperature gradient, the Fourier law is applied to calculate the thermal conductivity.

Complication exists in preparation of a reliable set of inter-atomic potentials between filler, polymer, and surface-coupling molecule for the MD simulation of the polymer composite material. In this thesis, we will firstly construct a set of inter-atomic potentials for a model polymer composite material with surface-coupling molecules. We will add an original inter-atomic potential that is based on the electronic density-functional theory to two suites of inter-atomic potentials for polymers and fillers, respectively. We will then perform the non-equilibrium MD simulation to obtain the temperature profile and heat flux in the system.

First of all, as for the situation of small packing fraction of fillers, we will investigate effects of the surface-coupling molecules on heat transfer by changing their lengths and density. We will show that the interfacial thermal conductance increases significantly by increasing either lengths or density of the SC molecules. We will investigate the atomistic details of the heat-transfer routes in the system. Secondly we will consider the situation of a high packing fraction of α-alumina fillers with/without the SC molecules. We will treat a system where a nanometer-depth polymer sub-system is sandwiched between two α-alumina slabs; that is, it contains two interfaces. We will perform a series of the NEMD runs by changing the polymer depth and adding the SC molecules to understand their effects on the interfacial thermal conductance. We will show that the interfacial thermal conductance is decreased significantly by decreasing the depth of the polymer sub-system without the SC molecules toward the chain-length of a bisA molecule, and that the interfacial thermal conductance is increased by adding the SC molecules. We will explain their microscopic mechanisms through combined analyses of the polymer configurations, atomic vibration spectra of the polymer sub-system [30,31], and phonon wave-packet dynamics simulation [32-35].

The rest of the present thesis is organized as follows. The following two sections in this chapter present a brief outline of the theory of interfacial thermal conductance and MD. In Chap. 2, atomistic modeling of the

simulation system and preparation of the inter-atomic potentials will be explained. Chapter 3 will report the effects of the surface-coupling molecules on heat transfer in the situation of small packing fraction of fillers. We will analyze size-effect on the thermal conductivity calculated with the NEMD simulation to set a proper size and temperature of the system for the present simulation and perform the NEMD runs at various settings of the surface-coupling molecules to understand their effects on the heat transfer. In Chap. 4, a series of the NEMD run at various settings of the polymer depth with/without the SC molecules to understand their effects on the interfacial thermal conductance. Chapter 5 will perform the atomic vibration spectra analysis through the equilibrium MD simulation to clarify the changes in the vibrational properties of the polymer sub-system by decreasing its depth and by adding the SC molecules. It will explain reasons for the changes in the interfacial thermal conductance obtained in Chap. 3. In addition, the phonon wave-packet dynamics simulation will perform to evaluate further the mode-dependent transmission coefficient through the interface and the group velocity in the polymer sub-system. The summary of the present study will be shown in Chap. 6

1.2 Interfacial thermal conductance

In this section, we introduce the basic theory of the interfacial thermal conductance and we discuss its relation with the phonon distribution at the interface. The rate of heat conduction through a medium in a specified direction (the $\mathbf{z}$-direction) is descried by Fourier's law for one-dimensional heat conduction as:

$$J = -\lambda \frac{\partial T}{\partial z}, \qquad (1.1)$$

where J is heat flux per unit area and λ is thermal conductivity of a material. Heat is conducted from high temperature to low temperature. The temperature gradient is negative when heat is conducted in the positive $\mathbf{z}$-direction.

As the study of thermal conductance between filler-polymer interface in the heat dissipation material, these interface can play a critical role in heat transfer because low interfacial thermal conductance between the filler and polymers. Even in nanometer scale interface (i.e., microscale voids do not exit), a temperature drop exists at the interface across the interface between two mediums by a heat flux as depicted in Fig 1.3. The physical origin of low interfacial thermal conductance cause that phonons are scattered partly at the interface not only by the differences in stiffness and mass density but also by the randomness and reconstructed structures. Phonons are quantized lattice vibrations that transfer heat and sound in a material. This finite phonon transmissivity gives rise to a temperature drop at the interface. The first experimental observation was reported by Kaptiza [11] who found that a finite temperature drop existed at the interface between He and a solid.

The interfacial thermal conductance G is described in terms of the ratio,

$$G = \frac{J}{T_a - T_b},$$

(1.2)

as the ratio between the heat flux per unit area J across an interface to the temperature drop ΔT at the interface as shows in Fig. 1.3. In general the heat flux is transmitted through a material by phonons (mainly in insulators) or electrons (mainly in metals) or other excitations as spin. In this study, we focus on the thermal conductivity by phonons because the heat dissipation materials, which are treated in this thesis, are electrically insulating.
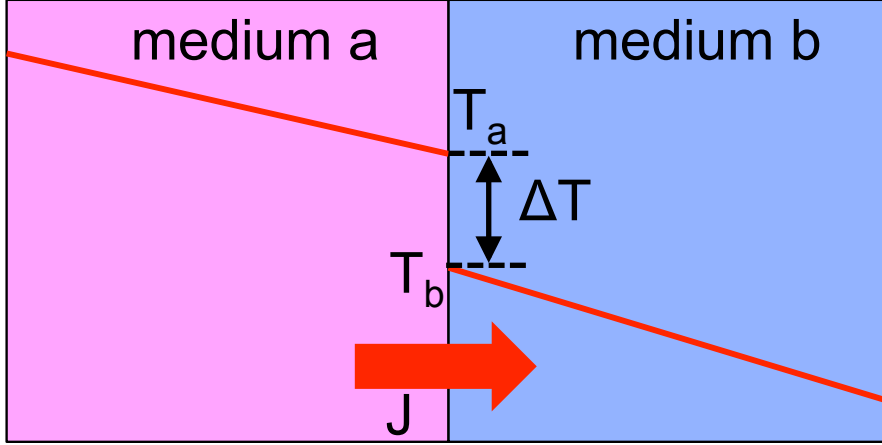
Figure 1.3: Schematic diagram of temperature drop ΔT at the interface between two medium crossed by heat flux J. The temperature profile in each medium is schematically represented by red solid lines.

The heat flux J per unit area across the interface (normal to z-direction) from medium-a at temperature $T = T_a$ to medium-b at $T = T_b$ is expressed in terms of transmitted phonons as

$$J = \frac{1}{V_a} \sum_{\text{mode},\vec{\eta}}^{+} v_{a,z}(\text{mode},\vec{\eta}) h f_a(\text{mode},\vec{\eta}) P_a(T_a,\text{mode},\vec{\eta}) t_{ab}(\text{mode},\vec{\eta})$$

$$+ \frac{1}{V_b} \sum_{\text{mode},\vec{\eta}}^{-} v_{b,z}(\text{mode},\vec{\eta}) h f_b(\text{mode},\vec{\eta}) P_b(T_b,\text{mode},\vec{\eta}) t_{ba}(\text{mode},\vec{\eta}) \, , \qquad (1.3)$$

with the volumes V's, phonon group velocities v's, phonon frequencies f's, phonon populations P's, and transmission coefficients t's. The summations are performed over the acoustic phonons, characterized with the wavelength vector $\vec{\eta}$ and transverse or longitudinal mode, in the first Brillouin zone with the direction of crossing the interface. We assume the principle of detailed balance in the situation where the two media are at thermal equilibrium at the common temperature T_a when the heat flux J vanishes. The two sums appearing in Eq. (1.3) can be reduced to a single sum on the phonon population coming from medium a. As for the interfacial thermal conductance, the Landauer formula[14,36] that uses the equilibrium phonon population (P) at the local temperature T_a, has commonly been used:

$G = (J/\Delta T)_{\text{Landauer}}$

$$= \frac{1}{V_a} \sum_{\text{mode},\vec{\eta}}^{+} v_{a,z}(\text{mode},\vec{\eta}) h f_a(\text{mode},\vec{\eta}) [dP_a(T_a,\text{mode},\vec{\eta})/dT_a] t_{ab}(\text{mode},\vec{\eta}). \quad (1.4)$$

Note that using the principle of detailed balance, the Landauer formula can be expressed as a function of the heat transport properties characterizing the medium b:

$G = (J/\Delta T)_{\text{Landauer}}$

$$= \frac{1}{V_b} \sum_{\text{mode},\vec{\eta}}^{-} v_{b,z}(\text{mode},\vec{\eta}) h f_b(\text{mode},\vec{\eta}) [dP_b(T_b,\text{mode},\vec{\eta})/dT_b] t_{ba}(\text{mode},\vec{\eta}) \quad (1.5)$$

1.3 Theoretical models for transmission coefficient

The behavior of heat carries incident on an interface is rather complex. A phonon incident on an interface might transmit or reflect, it could mode convert, or scatter into a different energy state, or couple to electrons. The transmission coefficient for a phonon can depend on its frequency, mode, angle of incidence, the density of phonon states in the materials, anharmonicity of interactions at the finite temperature, and the physical condition of the interface. Two theoretical models are well known: the acoustic mismatch model (AMM) [14-16] and the diffuse mismatch model (DMM) [17,18]. The AMM assumes that continuity of both displacement and stress at the interface gives all phonons reflect secularly with no scattering at the interface. In the DMM, the phonons scattered at the interface are assumed to lose fully the information of the incident directions.

1.3.1 Debye approximation

In this section, we assume Debye solids. In the Debye approximation, the group velocity of phonon is to be constant for each polarization type. The Debye velocity v_D is defined as

$$v_D = \frac{2v_\mathrm{t} + v_\mathrm{l}}{3}, \tag{1.6}$$

where the indexes t and l refer to the transverse and longitudinal polarizations, respectively. Under this assumption, the density of states is

$$g(f) = \frac{(2\pi f)^2}{2\pi^2 v_D^3}, \tag{1.7}$$

in the following we will drop the subscript "D".

1.3.2 Acoustic mismatch model

The AMM was proposed by Khalatnikov [15] and it was extended to apply for solid-solid interface by Little [16]. In the AMM, the degree of phonon reflection and refraction is determined by acoustic impedances Z_i where

$$Z_i = \rho_i v_i, \tag{1.8}$$

with the product of the mass density ρ_i.

The angles of phonon reflection at the interface and refraction on the other side are determined by the equivalent of Snell's Law.

$$\frac{sin\theta_a}{sin\theta_b} = \frac{v_a}{v_b}, \tag{1.9}$$

where θ_a is the angle of the incident phonon and θ_b is the refraction angle. the AMM transmission coefficient for the phonon with frequency in the common frequency range as

$$t_{ab}^\mathrm{AMM} = \frac{4Z_a Z_b \mu_a \mu_b}{(Z_a \mu_a + Z_b \mu_b)^2}, \tag{1.10}$$

where $\mu_i = cos\theta_i$. The AMM transmission coefficient is explained in detail in Appendix A. At high temperatures, we assume the equilibrium Bose-Einstein distribution $P_{eq}(f) \to k_B T/hf$, the AMM conductance which is calculated using the Landauer fomula Eq.(1.4) is expressed:

$$G_{eq}^\mathrm{AMM} = \frac{3}{2} n_a k_B v_a (\frac{v_b}{v_a})^3 \int_0^1 t_{ab}(\mu_a)\mu_a du_a, \tag{1.11}$$

where n_a denotes the number density of medium a. We have supposed without loss of generality that the medium denoted b has the lowest Debye

frequency. The factor $(v_b/v_a)^3$ comes from the phonon confinement of high frequency phonons in medium a. The interfacial thermal conductance with AMM Eq. (1.11) should be calculated numerically. If we assume that when the acoustic contrast between the two mediums is large, the transmission coefficient t_{ab} is dominated by phonons propagating with a small refraction angle (i.q., $\mu_2 \cong 1$). One can obtain easily analytical expressions for the AMM conductance. Under this approximation, the AMM conductance is given by the approximate form:

$$G_{eq}^{\text{AMM,appx}} = \frac{3}{2} n_a k_B v_a (\frac{v_b}{v_a})^3 I_1^{appx},$$ (1.12)

where I_a^{appx} using the acoustic ratio $\beta = Z_1/Z_2$:

$$I_1^{appx} = 4\beta(1 - \frac{\beta^2}{1+\beta} + \beta - 2\beta \log(\frac{1+\beta}{\beta})) .$$ (1.13)

The Eq.(1.12) is a very good approximation of the AMM conductance over a wide range of acoustic contrast [14]. The AMM model is supposed to predict the transmission of phonons of large wavelengths which behave as plane waves experiencing specular reflection or refraction at the interface. This model is commonly thought to apply at low temperatures where only long-wavelength phonons are populated.

1.3.3 Diffuse mismatch model

At higher temperatures, interfacial scattering is thought to be diffuse essentially because most of wavelengths of phonons become smaller than the interfacial roughness and high frequency phonons dominate the heat flux. For high frequency phonons, the physical and chemical roughness at the interface becomes comparable to the wavelength of the dominant heat carrying phonons, making phonon reflection and transmission less specular. Therefore, the AMM does not express heat transfer that well at higher temperatures. To address this issue, the DMM proposed by Swartz and Pohl [12,18]. In the DMM, the phonons scattered at the interface are assumed to lose fully the information of the incident directions. The DMM assumes elastic scattering at the interface and thus the frequency of the phonon does

not change during scattering at the interface. As a result, the transmission coefficient depends only on the phonon density of states on the both side of the interface with satisfying the principle of detailed balance. The assumption of the DMM suppose to the phonon reflectivity from medium a to medium b equals the transmission coefficient from medium b to medium a, as follows:

$$1 - t_{ab} = t_{ba}.$$ (1.14)

Combining Eq. (1.14) with the principle of detailed balance of energy flux for each f under the thermal equilibrium as follow

$$v_{a,z}P_a t_{ab} = v_{b,z}P_b t_{ba},$$ (1.15)

an expression for t_{ab} can be obtained. We assume Debye approximation for the phonon dispersion relation, which leads to the following transmission coefficient with the phonon density-of-state $g_i(f)$.

$$t_{ab}^{\text{DMM}} = \frac{v_b g_b(f)}{v_a g_a(f) + v_b g_b(f)}.$$ (1.16)

Since the transmission coefficient does not depend on the incident angle, the DMM conductance has a simple expression:

$$G_{eq}^{\text{DMM}} = \frac{3}{4} n_1 k_B \frac{v_b^2}{v_a^2 + v_b^2}.$$ (1.17)

At higher temperatures, the DMM conductance tends to agree well with experimentally observed interfacial thermal conductance compared to the AMM. One possible explanation for interfacial thermal conductance G is the discontinuity in the phonon density of states across the interface. At higher temperatures where a full spectrum of vibrational modes is thermally excited, the measured interfacial thermal conductance is in poor agreement with the theoretical models.

1.3.4 Non-equilibrium effect

Limitations of the Landauer formula are well known, including the paradox that the formula gives a finite conductance even for the virtual interface

with identical sub-systems [13,14,29,37]. The paradox is due to ignorance of non-equilibrium nature of P, that is, the P at a given location should be affected by the ones within the range of the phonon mean free-path. The interfacial thermal conductance by accounting non-equilibrium effect G_{neq} predict larger than G_{eq}. If we consider identical materials, interfacial conductance Eq. (1.4) becomes infinity. The G_{neq} solves the paradox of the interfacial thermal conductance between identical materials.

In this thesis, the non-equilibrium effect in detail is not discussed. We just introduce the thermal conductance expression with accounting the non-equilibrium effect. The interfacial thermal conductanc G_{neq} with AMM transmission coefficient is

$$G_{neq}^{\text{AMM}} = \frac{G_{eq}^{\text{AMM}}}{1 - \frac{3}{2}\frac{v_b}{v_a}\left(\int_0^1 \mu_a^2\, t_{ab}(\mu_a)du_a + \frac{c_b}{c_a}\int_0^1\int_0^1 \mu_a\,\mu_b t_{ab}(\mu_a)du_a\right)}, \qquad (1.18)$$

where μ_b is the cosine of the refracted angle. The formula Eq. (1.18) can be approximated

$$G_{neq}^{\text{AMM,appx}} = \frac{G_{eq}^{\text{AMM,appx}}}{1 - \frac{3}{2}\frac{v_b}{v_a}(I_2^{appx} + \frac{c_b}{c_a}I_3^{appx})}, \qquad (1.19)$$

where $I_3^{appx} = I_1^{appx}$ in Eq.(1.19) and

$$I_2^{appx} = 4\beta(\frac{1}{2} - 2\beta - \beta^2 + \frac{\beta^3}{1+\beta} + 3\beta^2\log(\frac{1+\beta}{\beta})). \qquad (1.20)$$

The interfacial thermal conductance obtained using the DMM transmission coefficient is

$$G_{neq}^{\text{DMM}} = \frac{G_{eq}^{\text{DMM}}}{1 - (v_a v_b + v_b^2)/2(v_a^2 + v_b^2)}. \qquad (1.21)$$

1.4 Molecular Dynamics simulation

This chapter presents an overview of the Molecular Dynamics (MD) simulation to study thermal transport properties. There are two main families of MD methods. One is the classical MD and other is first principle MD. In this section, we focus on classical MD only and the classical MD is simply referred to as MD.

1.4.1 Molecular dynamics

The MD is one of the most basic techniques for computer simulation of complex systems at the atomistic level. Due to the advances in computer technology and algorithmic improvements, MD has become an important tool in many fields of physics and chemistry. The most important point of the MD scheme is how to describe the interatomic interaction, or how to incorporate electronic structural change as a hidden variation. In MD, it is hard to deal with a quantum effects such as changes in chemical bonding, the presence of important noncovalent intermediates and tunnelling of protons or electrons. The first-principles MD simulation method with interatomic interaction calculated on the fly from the electronic structure. However the first-principles MD require more computational costs. In this thesis, we deal with complex systems such as an interface and to obtain thermal conductivity take over time scales of nanoseconds. The MD is suited for these situations. The MD method, which uses potentials based on experimental data or the independent electronic structure calculation is popular. The interaction is usually divided into two-body, three-body, and many-body terms, they may be long-ranged or short-ranged; each term is represented by a useful function form. Ideally empirical potentials should also be transferable and applicable to possibly many systems under different conditions. In Chap 2.2, we describe interatomic interactions which are used in this study.

The MD is a simulation method based on the numerical integration of Newton's equation of motion:

$$m_i \frac{d^2 \vec{r_i}(t)}{dt^2} = \vec{F_i}, \tag{1.22}$$

where: $\vec{r_i}(t) = (x_i(t), y_i(t), z_i(t))$ is the position vector of atom i, $\vec{F_i}$ is the force vector and m_i is the mass of atom. To integrate the above second-order differential equations the instantaneous forces acting on the atoms. The MD simulation begins by initialization of the atomic positions and velocities. For a crystal solid, for example, the initial positions will be determined by an atomic position in the unit cell and its spatial copies in the crystal symmetry. Then the simulation cell contains the repeated unit cells. For an amorphous solid such as polymers, for instance, molecules added into a three-dimensional cell and these conformations and positions are optimized to realize energy minimum in the cell through a Monte Carlo method. The initial velocities are often chosen randomly from a Maxwell-Boltzmann or Gaussian distribution at a given temperature, which gives the probability that an atom i has a velocity v_i

$$f(v_i) = \left(\frac{m_i}{2\pi k_B T} \right) exp \left[-\frac{1}{2} \frac{m_i v_i^2}{k_B T} \right], \tag{1.23}$$

where k_B is Boltzmann constant, T is temperature under the condition that total atomic momenta are zero. When this initialization is made for given temperature once, total energy of the system is conserved. The instantaneous temperature $T(t)$ with atomic mass m_i and velocity v_i of atom i is defined in the following:

$$\frac{3}{2} N k_B T(t) = \sum_{i=1}^{N} \frac{m_i v_i^2}{2}, \tag{1.24}$$

where N represents the number of atoms in simulation system.

The MD algorithm to be mentioned in the next subsection has the time reversal symmetry. Therefore, unlike the Monte Carlo method, if a set of positions and velocities is given first, MD is a deterministic method in that the time evolution is completely determined from its current state. Statistical mechanics is used in order to extract macroscopic information from the microscopic one provided by the MD simulations. It is based on the concept that many individual microscopic configurations in a large system

lead to the same macroscopic properties after long time simulations. In other words, it is not necessary to save all the detailed trajectories of every particle (atom) in the system in order to predict the physical properties. Usually the statistical ensemble is characterized by fixing the thermodynamic variables (e.g., total energy E, temperature T, pressure P, volume V, number of atoms N, or chemical potential u). There are various types of statistical ensembles depending on variables kept fixed. The microcanonical ensemble is characterized by constant N, V, and E, and denoted as NVE ensemble. Other important ensembles include the canonical (NVT) ensemble, the isothermal-isobaric or NPT ensemble, and the grand-canonical (uVT) ensemble. The thermodynamic variables which define an ensemble can be considered as control parameters when a simulation run is carried out.

1.4.2 Time integration of equation of motion

Owing to the many-body nature of the problem, the equations of motion are discretized and solved numerically. The positions and velocities define the MD trajectories. The MD trajectories describe the time evolution of the system. Accordingly, the positions and velocities are propagated with a finite time interval using numerical integrators. Various techniques to integrate the equation of motion have been developed. The Verlet method is commonly used because its simplicity and stability [38]. Assume that forward and backward of position x in time are represented by the Taylor expansion as follows:

$$x(t + \delta t) = x(t) + v(t)\delta t + \frac{F(t)}{2m}\delta t^2 + \cdots, \qquad (1.25)$$

$$x(t - \delta t) = x(t) - v(t)\delta t + \frac{F(t)}{2m}\delta t^2 - \cdots, \qquad (1.26)$$

where v is velocity and F denotes force. Adding the two expression gives

$$x(t + \delta t) = 2x(t) - x(t - \delta t) + \frac{F(t)}{m}\delta t^2 + \cdots, \qquad (1.25)$$

notice that the velocity does not explicitly appear in the Verlet algorithm.

This may be a problem if properties of the system that depend on velocity, such as kinetic energy, are desired. To overcome this problem, some variants of the Verlet algorithm have been developed. The Velocity Verlet algorithm simultaneously updates positions and velocities. The positions are represented Eq. (1.25) and The velocity are expressd as

$$v(t + \delta t) = v(t) + \frac{F(t)}{m} \delta t + \cdots,$$ (1.26)

$$v(t) = v(t + \delta t) - \frac{F(t + \delta t)}{m} \delta t + \cdots.$$ (1.27)

These equations lead to following formula:

$$v(t + \delta t) = v(t) + \frac{F(t + \delta t) + F(t)}{2m} \delta t.$$ (1.28)

When initial position $x(0)$ and velocity $v(0)$ are given, their time evolutions are obtained by updating a time step to $x(t + \delta t)$, $F(t + \delta t)$, and $v(t + \delta t)$.

1.4.3 Velocity scaling

To calculate thermal transport properties, we use the non-equilibrium MD. In the NEMD, a heat flux is applied to a simulation cell along the direction of interest by controlling temperature. Controlling temperature to T_{req} is realized by the direct velocity scaling. Direct velocity scaling is a drastic way to change the velocities of the atoms so that the target temperature T_{req} can be exactly matched whenever the system temperature is lower or higher than the target by some user-defined amount. That is each atomic velocity v' is multiplied by the same factor α

$$v' = \alpha \cdot v \; with \; \alpha = \sqrt{\frac{T_{req}}{T(t)}}.$$ (1.29)

Chapter 2

Modeling of system and preparation of inter-atomic potentials

2.1 Modeling of system

In the present simulation study, we assume α-alumina for the filler and bisphenol-A (bisA) epoxy for the polymer (see, Fig. 2.1(a)) because both are commonly used for the electrically insulating heat-dissipation composite material [2,39,40]. Figure 2.1 (a) shows the present model of the bisA molecule, in which two epoxy groups terminate the two ends. It is known experimentally that various degrees of polymerization through bonding reaction of the epoxy groups occur for the bisA molecules [41]. However, we here take the simplest model (Fig. 2.1) from the following reasons: (i) Irrespective of the degree of polymerization, two epoxy groups remain at the two ends. (ii) Essential physics are expected to depend on the ratio of the chain length of a bisA molecule to the depth of the polymer sub-system. (iii) Recent papers have used the present simple model as a fundamental one for the cross-link reactions [42,43].

For the surface-coupling agent, the silane composite molecule is often used. The silane composite molecule is basically composed of two kinds of groups attached to a Si atom: the reaction group (e.g., epoxy) bonds to an organic polymer, while the OR group (e.g., -O-CH$_3$) undergoes the hydrolysis
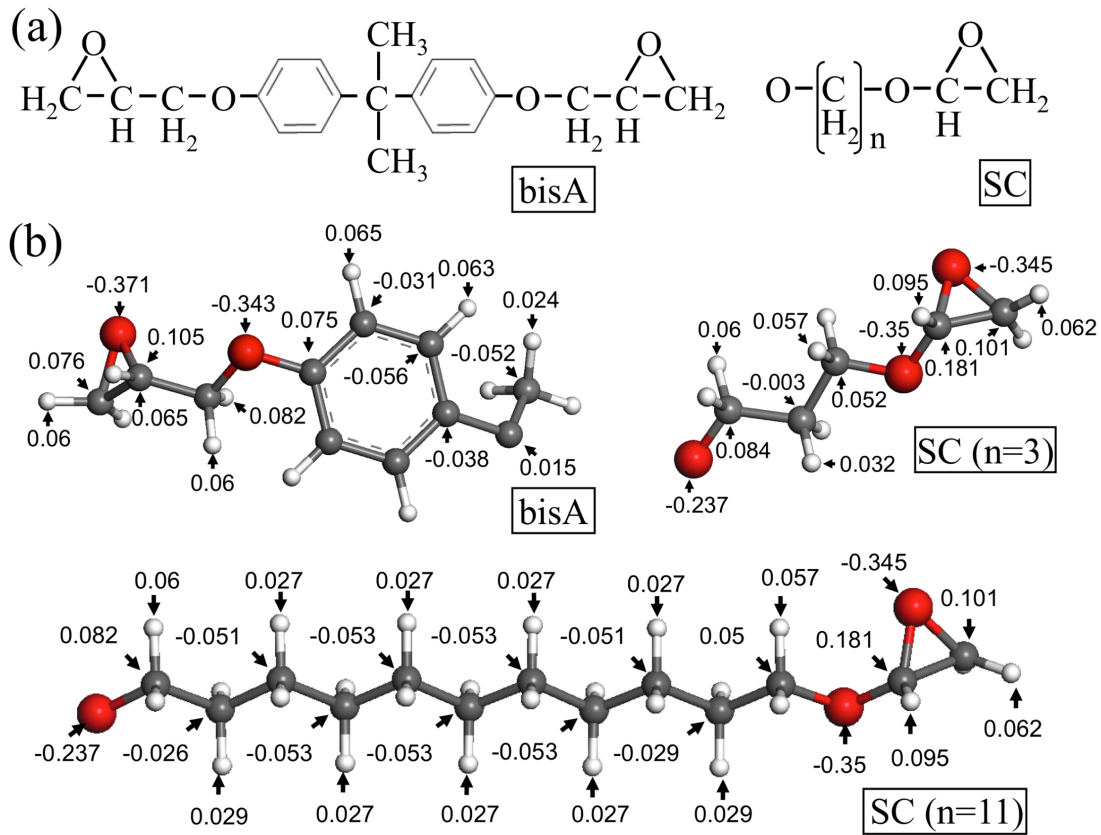
Figure 2.1: (a) Structure of bisphenol-A (bisA) and model SC molecules. (b) Atomic charges in unit of e of the bisA molecule (equivalent atoms are omitted for symmetry) and SC molecules with n = 3 and 11.

reaction to form a strong bond between the O and a surface atom of an inorganic filler [10]. The silane composite molecule thereby works to bind a filler and polymer together. In the present simulation we use a virtual surface-coupling (SC) molecule shown in Fig. 2.1 that mimics the state after the hydrolysis reaction: an epoxy group connects to $(CH_2)_n$ while the other end of $(CH_2)_n$ is saturated with an O atom. We set n of $(CH_2)_n$ to either 3 or 11. The chain-lengths of bisA is about $20\,\text{Å}$ and the chain-lengths of SC molecules are $8\,\text{Å}$ and $20\,\text{Å}$ for n=3 and 11 of $(CH_2)_n$.

In the present simulation we use a virtual surface-coupling (SC) molecule shown in Fig. 2.1 that mimics the state after the hydrolysis reaction: an epoxy group connects to $(CH_2)_n$ while the other end of $(CH_2)_n$ is saturated with an O atom. We set n of $(CH_2)_n$ to either 3 or 11. The chain-lengths of bisA is about $20\,\text{Å}$ and the chain-lengths of SC molecules are $8\,\text{Å}$ and $20\,\text{Å}$ for n=3 and 11 of $(CH_2)_n$.

2.2 Inter atomic potential

We use the following form of two-body inter-atomic interaction potentials for Al and O in α-alumina in the CMAS potential suite [44]:

$$E(r_{ij}) = \frac{q_i q_j}{r_{ij}} - C_i C_j \left(\frac{1}{r_{ij}}\right)^6 + (B_i + B_j) f \exp\left(\frac{A_i + A_j - r_{ij}}{B_i + B_j}\right) \tag{2.1}$$

with the atomic charges $\{q_i\}$ and parameters $\{A_i\}, \{B_i\}, \{C_i\},$ and f. The suite has been widely used for the MD simulation of MgO, CaO, alumina, and SiO₂ systems. Parameters used in alumina are shown in Table 2.1. The Dreiding inter-atomic potentials [45] are applied to the bisA and SC molecules

$$E = \sum_{(i,j)} \frac{K_{ij}}{2} (r_{ij} - r_{ij,\text{eq}})^2 + \sum_{(i,j,k)} K_{ijk} (\theta_{ijk} - \theta_{ijk,\text{eq}})^2$$

$$+ \sum_{(i,j,k,l)} \frac{V_{jk}}{2} \{1 - \cos[n_{jk}(\varphi_{ijkl} - \varphi_{ijkl,\text{eq}})]\}$$

$$+ \sum_{(i,j)} \sqrt{\epsilon_i \epsilon_j} \left[\left(\frac{\sigma_i + \sigma_j}{2r_{ij}}\right)^{12} - \left(\frac{\sigma_i + \sigma_j}{2r_{ij}}\right)^6\right] + \sum_{(i,j)} \frac{q_i q_j}{r_{ij}} \tag{2.2}$$

with the atomic charges $\{q_i\}$ and various parameters $\{K_{ij}\}$, $\{K_{ijk}\}$, $\{V_{jk}\}$, $\{r_{ij,\text{eq}}\}, \{\theta_{ijk,\text{eq}}\}, \{n_{jk}\}, \{\varphi_{ijkl,\text{eq}}\}, \{\epsilon_i\},$ and $\{\sigma_i\}$. In Eq. (2.1), the bonded inter-atomic interaction is described by the two-body bonding, three-body angle, and four-body torsion terms, while the non-bonded one by the van der Waals and Coulomb terms; the non-bonded interaction with up to the third nearest neighbor atoms is omitted. Table 2.2 shows parameters of the Dreiding inter-atomic potentials, which are used in this study. As a bisA or SC molecule, O atoms are divided into O_R (bonded benzene) and O_3 (others); C atoms, into C_R (benzene) and C_3 (others). We need to

determine the atomic charges $\{q_i\}$ in Eq. (2.1) for the bisA and SC molecules. Following the Gasteiger-Marsili method [46], we obtain the charges as solutions to a set of generalized electronegativity equalization equations for the corresponding sigma-bond model system for each kind of molecules. The calculated values of the charges are typed in Fig. 2.1(b).

We need to construct the inter-atomic potential between the SC molecule and α-alumina. To calculate the energies at various configurations of them we use the DMol³ software package [47,48] in Materials Studio 5.5 with the PBE [49] form of the generalized gradient approximation for the exchange-correlation potential. The energy tolerance in the self-consistency field iteration is set to 5×10^{-5} eV per atom. As for the basis set for the electron orbitals, we use the double numerical with polarization (DNP) set recommended in the DMol³ for high accuracy purposes. As an accuracy check, we calculate the cohesion energy of bulk α-alumina to find 2.6 eV per Al-O bond and the elastic constants $C_{11} = 518$ GPa and $C_{33} = 494$ GPa .Their differences from the experimental values are as small as 5 % [50,51].

We consider (0001) surface of α-alumina as the filler surface, which is the most stable one when terminated with Al [52-54]. As depicted in Fig. 2.2, a thin α-alumina slab of 120 atoms with (0001) surface is placed in the rectangular parallelepiped of $(L_x, L_y, L_z) = (14.0\,\text{Å}, 8.2\,\text{Å}, 7.0\,\text{Å})$; the vacuum layer with z-depth 20 Å is added on the (0001) surface. The periodic boundary conditions are applied in the three directions. Using the DMol³ package, geometry optimization is performed for the system. The outermost Al atoms sink to lie nearly on the same O-plane as reported in a former paper [52]. We then place a single SC molecule on the (0001) surface to find the most stable configuration. Figure 2.2(a) depicts the most stable configuration obtained through the relaxation runs starting with various settings of the SC molecule including the case with 45 degrees inclined toward the (0001) surface. We find that the O atom at the end of the SC molecule bonds tightly to a surface Al atom.

The binding energy, which is defined as the difference in the total energy between the well-separated and ground-state configurations, is 2.06 eV; the
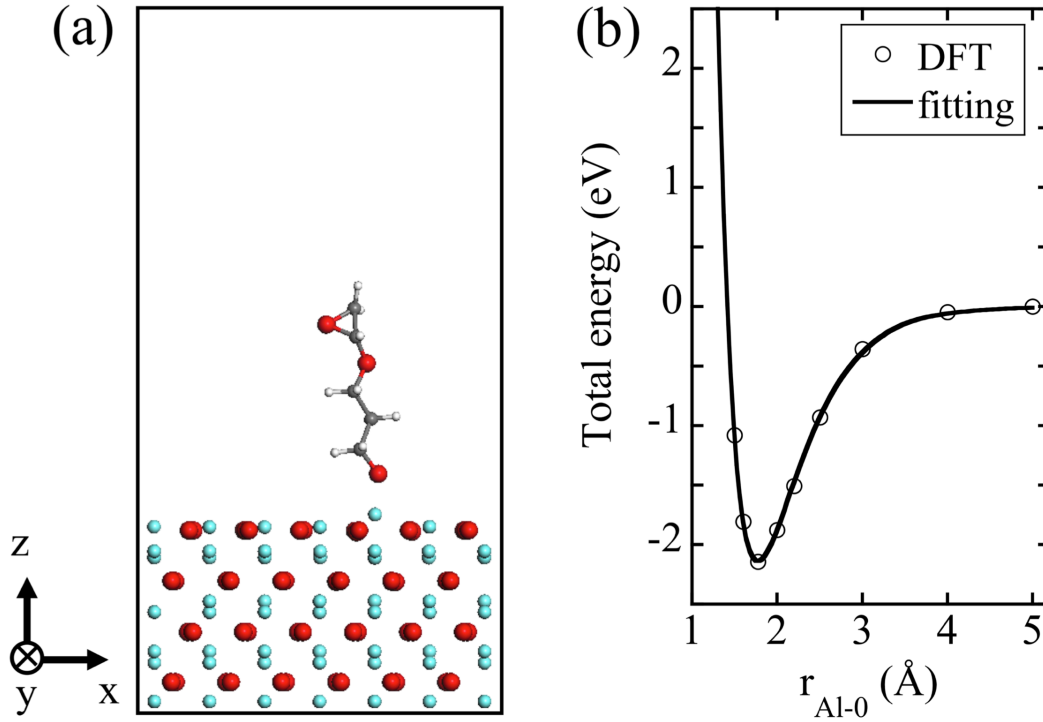
Figure 2. 2: (a) Ground-state configuration of a SC molecule on (0001) surface of α-alumina. Large red spheres are O; small cyan, Al; medium grey, C; small white, H. (b) Total energy of the system in (a) as a function of r_{Al_O}

Al-O distance $r_{Al-O} = 1.77$ Å. The binding energy is smaller by 20 % than the cohesive energy per Al-O bond of bulk α-alumina; the r_{Al-O} is shorter by $0.1 - 0.2$ Å than the average in bulk α-alumina. Figure 2.2(b) shows the total energy minus the value at $r_{Al-O} = 5.0$ Å as a function of r_{Al-O}; for each value of r_{Al-O}, all the other atoms are relaxed. We fit the calculated energies to the Morse potential form:

$$E(r_{Al-O}) = D_e\{1 - \exp[-\Upsilon(r_{Al-O} - r_{Al-O,eq})]\}^2 - D_e \qquad (2.3)$$

with $D_e = 2.06$ eV, $r_{Al-O,eq} = 1.77$ Å, and $\Upsilon = 1.93$ Å^{-1}

For the inter-atomic interaction between α-alumina and SC molecules and between α-alumina and bisA molecules, we firstly adopt the van der Waals and Coulomb terms in Eqs. (2.1) and (2.2) with the same parameter values for pure α-alumina, SC, and bisA systems. For each bonding pair of Al atom of α-alumina and O atom of the SC molecule, we then subtract the van der Waals and Coulomb terms and apply Eq. (2.3).

Table 2.1: Parameters of CMAS potential.

Atomic type	q [e]	A [Å]	B [Å]	C [Å^3(kcal/mol)$^{1/2}$]	f [kcal/(Å·mol)]
Al	1.4175	0.7852	0.034	18.001	1
O	-0.945	1.8215	0.138	44.2976	1

Table 2.2: Parameters of Dreiding potential.

2.2.1: Two body bonding term

i	j	r_{ij_eq}[Å]	K_{ij}[kcal/(Å·mol)]
C_3	C_3	1.53	700
C_3	C_R	1.46	700
C_3	O_3	1.42	700
C_3	O_R	1.42	700
C_3	H	1.09	700
C_R	C_R	1.39	1050
C_R	O_R	1.35	1050
C_R	H	1.02	700

2.2.2: Three body angle term

i	j	k	$\theta_{ijk,eq}$[dgrees]	K_{ijk}[kcal/(mol·rad^2)]
*	C_3	*	109.471	100
*	C_R	*	120	100
*	O_3	*	104.51	100
*	O_R	*	120	100

2.2.3: Four body torsion term

i	j	k	l	V_{jk}[kcal/mol]	$\varphi_{ijkl,\text{eq}}$[degree]	n_{jk}
C_R	C_R	C_3	*	1	0	6
C_R	O_R	C_3	*	1	0	6
*	C_3	C_3	*	2	180	3
*	C_R	C_R	*	25	0	2
*	O_3	C_3	*	2	180	3
*	O_R	C_R	*	25	0	2

2.2.4: Van der Waals term

Material	Atomic type	σ_i[Å]	ε_i[kcal/mol)]
Al_2O_3	Al	4.390	0.31
	O	3.4046	0.0957
bisA or	C_R	3.8983	0.0951
SC	O_3	3.4046	0.0957
	O_R	3.4046	0.0957
	H	3.1950	0.0152

Chapter 3

The situation of small packing fraction of fillers

In Chap. 3, we consider the alumina-polymer-alumina system for the situation of small packing fraction of fillers. We investigate effects of the surface-coupling molecules on heat transfer by changing their lengths and density though the non-equilibrium MD. We calculate the effective thermal conductivity of the interface area using the heat flux, surface area, and temperature profile (or time-averaged kinetic energies) in the system. In the NEMD, we control kinetic energies of those atoms at the temperature-controlled area to obtain the heat flux. We assume thermal equilibrium at an area away from the temperature-controlled one. In a simulation run we confirm that the system is in the steady state by comparing the input and output energies in the temperature-controlled areas. In addition we discuss the atomistic details of the heat-transfer routes in the system. We calculate the time-averaged kinetic energies (or atomic temperatures) of atoms in the non-equilibrium run. The heat transfer routes are therewith identified under the assumption that the difference in the atomic temperatures of a pair of atoms gets smaller as the degree of thermal conductance between the two atoms becomes smaller. We identify the energy (or heat) transfer routes around the interface and we find key heat-transfer routes that involve the surface-coupling molecules.

3.1 Setting in NEND

3.1.1 Model size of the system

A simulation system is depicted in Fig. 3.1. The periodic boundary conditions are applied in the three directions. To obtain thermal conductance of the system, we control the temperatures of the center (bisA) and two ends (α-alumina) of the system to low and high values, respectively, as shown in Fig. 3.1, we produce heat fluxes that direct from the α-alumina to bisA regions.

First we need to determine the proper size of the simulation system from following analyses. It has been remarked that the thermal conductivity of a bulk material calculated using the non-equilibrium MD simulation method often shows a significant system-size dependence [20,23,32]. In the method, two well-separated slab areas in the system are controlled to different temperatures. The input and output fluxes of heat at the temperature-controlled areas are calculated in the steady state. Using the temperature gradient at a proper position, the heat flux, and the distance between the areas, we calculate the thermal conductivity (see, Eq. 3.1 below). If the system size is shorter than the mean free-path of phonons, the thermal conductivity is underestimated because the phonons are scattered artificially at the temperature-controlled areas [20,23,32]. In the present simulation of the interface system containing α-alumina and bisA regions, changing the width of the α-alumina region gives no significant effect on the overall thermal resistance of the system because the thermal resistance of bisA is much higher than that of α-alumina. In the following, we determine the width of the bisA region heuristically by performing separately various non-equilibrium MD runs for pure bisA systems.

We prepare the bisA systems with $\left(L_x, L_y, L_z\right) = (34\,\text{Å}, 38\,\text{Å}, 62\,\text{Å})$, $(34\,\text{Å}, 38\,\text{Å}, 112\,\text{Å})$, and $(34\,\text{Å}, 38\,\text{Å}, 224\,\text{Å})$ under the periodic boundary conditions to perform the non-equilibrium MD simulation runs. In the three systems, the bisA molecules form amorphous solids with the same mass
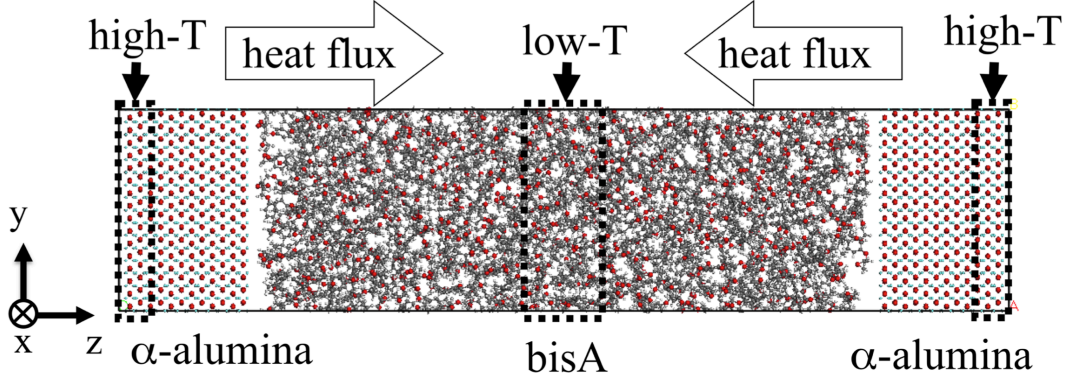
Figure 3.1: Atomic configuration of the system with no SC molecule in the present simulation.

density of $0.90\,\text{g/cm}^3$. The average temperatures of the system are $T = 300\,\text{K}$, $400\,\text{K}$, and $500\,\text{K}$. The two ends of the system are controlled to $T + 20\,\text{K}$, while the central area to $T - 20\,\text{K}$. Since the bisA molecules diffuse slightly at those temperatures, the number of atoms located in each temperature-control area with 6.2 Å z-width fluctuates in time (for instance, $600 - 700$ in the low-temperature control area in the run at $T = 500\,\text{K}$) but shows no tendency of drift after 0.1 ns. We use the temperature profile at a z-range that is well separated (> 10 Å) from the temperature-control areas to obtain a reliable value for the thermal conductivity. At $T = 300\,\text{K}$, the thermal conductivities are calculated as 0.07, 0.08, and $0.12\,\text{W/m} \cdot \text{K}$ for the cases with $L_z = 62\,\text{Å}$, $112\,\text{Å}$, and $224\,\text{Å}$, respectively. The present value, $0.12\,\text{W/m} \cdot \text{K}$, of the thermal conductivity for the case of $L_z = 224\,\text{Å}$ is close to the experimental values in the range of $0.15 - 0.25\,\text{W/m} \cdot \text{K}$ at room temperatures [7]. At $T = 400\,\text{K}$ and $500\,\text{K}$, the thermal conductivity appears to be saturated to $0.11 - 0.13\,\text{W/m} \cdot \text{K}$ for $L_z \geq 112\,\text{Å}$. It is confirmed that increasing the temperature difference between the two ends to 60 K gives the same value within error bars for the thermal conductivity. Considering those, we set the z-width of the bisA region to $112\,\text{Å}$ and the system temperature to $T = 400\,\text{K}$ with plus 30 and minus 30 K at the temperature-control areas in the present simulation runs.

3.1.2 Simulation system for thermal conductivity

A typical configuration of the system in the present non-equilibrium MD simulation is depicted in Fig. 3.1. It corresponds to the case with no SC molecule. The periodic boundary conditions are applied in the three directions. The system is a rectangular parallelepiped with dimensions $(L_x, L_y, L_z) = (34\,\text{Å}, 38\,\text{Å}, 168\,\text{Å})$; it is composed of 18,656 atoms. The left and right 6.2 Å z-width ends are controlled to $T = 430$ K, while the central 12.4 Å z-width to $T = 370$ K. The simulation system contains the bisA region with 112 Å in z-width at the center, which is sandwiched in z-direction between the α-alumina regions. Note that the α-alumina regions are connected to each other from the periodicity of the system. In a simulation run, the velocity-Verlet algorithm [38] is used to integrate the equations of motion. The temperature is controlled with the simple velocity-scaling method. We set the time step $dt = 1.0$ fs from detailed analyses about the dt-dependencies of the temperature profile and energy flux for a practical system, which will be explained in Chap. 3.3.

By controlling the temperatures of the center (bisA) and two ends (α-alumina) of the system to low and high values, respectively, as shown in Fig. 3.1, we produce heat fluxes that direct from the α-alumina to bisA regions. We calculate the effective thermal conductivity Λ of the system after the steady state is realized as

$$\Lambda = \frac{Jl}{T_1 - T_2},$$
(3.1)

where J is the heat flux per unit time and surface area, T_1 and T_2 are the high and low temperatures of well-separated z-positions under the condition that both are not close to the temperature-control areas, and l is the distance between the high- and low-temperature positions. In a simulation run we confirm that the system is in the steady state after 1.5 ns by comparing the input and output energies per unit time in the temperature-controlled bins. The J and temperature profile are obtained as averages over 0.5 ns in the steady state.

3.1.3 Time-step and calculate temperature profile

We here add the SC molecules to the system to analyze their effects on heat transfer through the interface. For the analyses we need to compare the results for various settings of the SC molecules. For $n = 3$ of $(CH_2)_n$ of the SC molecule, number of the SC molecules in the system is {1, 4, 8, 16, 32}. For $n = 11$, the number of the SC molecules is 16. We arrange the SC molecules that bond to surface Al atoms in a square-lattice form as depicted in Fig. 3.2; such Al-O bonds are kept during a run. At the addition of the SC molecules we need to increase L_z of the system from the original value of $L_z = 168$ Å (no SC molecule) so that the averaged mass density does not change from 1.85 g/cm^3. Even when SC molecules are added, the system became equilibrium structurally in a relatively short time because constituent elements and the structure of SC molecule are similar to the bisA molecule's (see Fig.2.1). To prevent sharp a local stress change, the mass density of the polymer is altered gradually.

We set the time step, dt, to a proper value by comparing simulation results for a typical system between with $dt = 0.5$ and 1.0 fs. For the purpose, the case of containing a 16 SC molecules with $n = 3$, denoted as M16n3, is considered. Figure 3.3 (a) depicts the energy fluxes, J, in the two runs; the positive values correspond to the input fluxes to the high-temperature control area, while the negative values to the output fluxes from the low-temperature control area. Even with $dt = 1.0$ fs, the input and output fluxes agree well with each other indicating no system heat-up. Figure 3.3(b) shows the temperature profile of the bisA region in the system. We here consider the bisA region only because the temperature profile is flat in the α-alumina region (see, Fig. 3.4). The temperature profile in Fig. 3.3 (b) is obtained as the average of two profiles with the z measuring from the center to the left and right of the system, respectively (see, Fig. 3.1). The α-alumina region correspond to $z = 0 - 26$ Å. The low-temperature control area corresponds to $z = 70 - 85$ Å. We find in Fig. 3.3 (b) that the temperatures calculated for all atoms in the 1.0 fs run deviate substantially from the
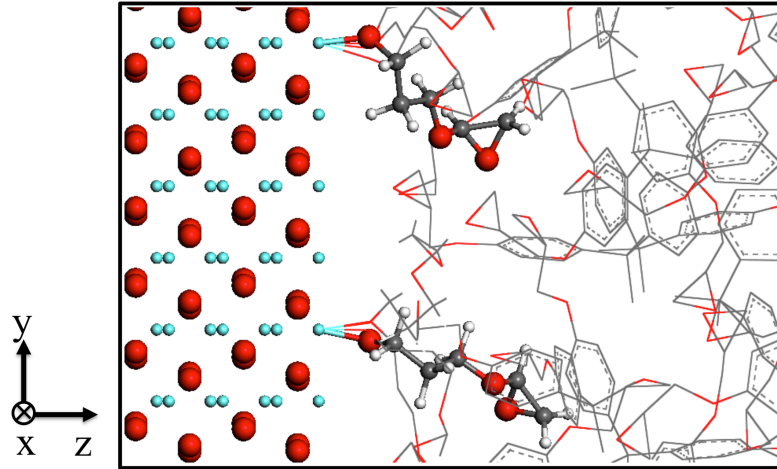
Figure 3.2: Atomic configuration of SC molecules on (0001) surface of α-alumina in the M16n3 case viewed from x-direction. Large red spheres are O; small cyan, Al; medium grey, C; small white, H. The bisA molecules are drawn by sticks.

reference ones in the 0.5 fs run. Interestingly, however, the temperatures calculated without H atoms in the 1.0 fs run agree well with the reference ones as seen in Fig. 3.3 (b). Since the calculated temperatures change little (< 1.3 K) if we omit H atoms in the 0.5 fs run, we consider that such a substantial temperature change seen in the 1.0 fs run is related to the fast vibration of H. From those observations about the J and temperature profile, we choose to set $dt = 1.0$ fs for fast simulation and omit H atoms to calculate the temperature profile.
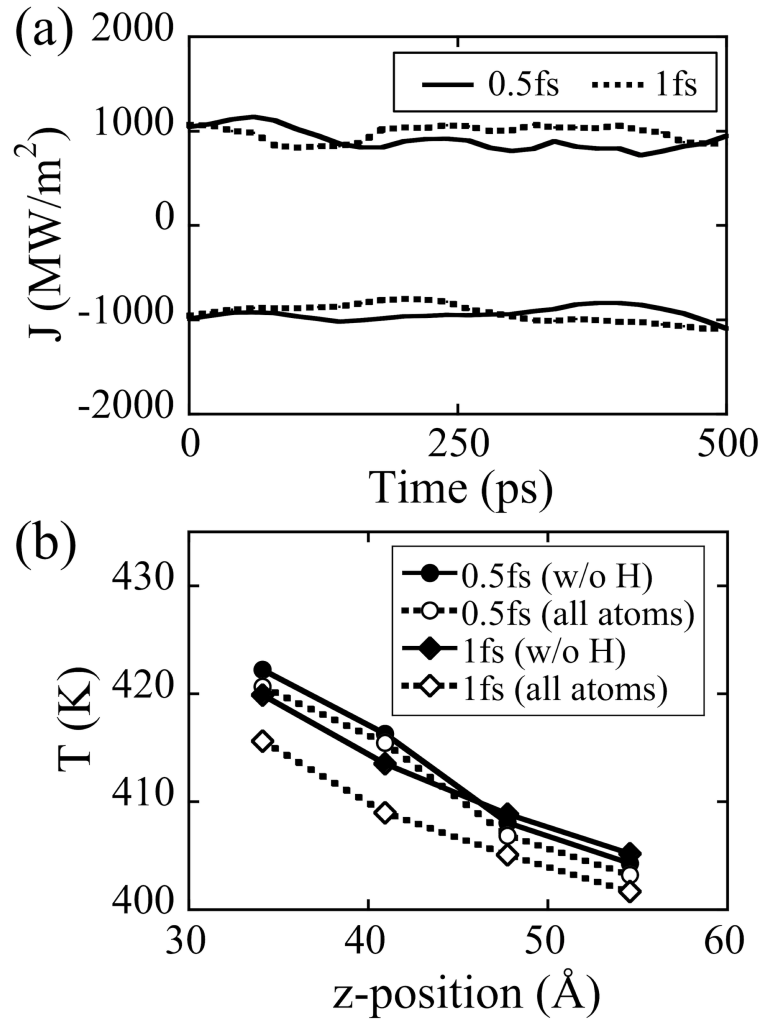
Figure. 3.3: (a) Time evolution of J in the high- and low-temperature control areas for the M1n3 case. The solid curve corresponds to the time step 0.5 fs; dotted curve, to 1.0 fs. (b) Temperature profiles in the bisA with SC region in the M1n3 case. The profiles are calculated either for all atoms (open symbols) or without H (filled symbols).

3.2 Result and discussion

3.2.1 Thermal conductivity and interfacial thermal conductance

Figure 3.4 shows the detailed temperature profiles (top) and snapshots of atomic temperatures (bottom) in two typical cases: one is the M16n3 case and the other is the case of a single SC molecule with $n = 3$ denoted as M1n3. The dashed line in temperature profiles in Fig. 3.4 (top) represents the extrapolation of the two data points near the interface in the bisA region. Since the end z-position of the bisA with SC region fluctuates in time and varies depending on the x-y location, we set it as the one separated by 2.0 Å from the end (i.e., Al) of α-alumina, therefore at $z = 28$ Å. We use $z = 28$ Å to predict the local temperature of the bisA with SC region at the interface. The temperature profiles are almost flat in the α-alumina region, while linearly decreasing profiles are seen in the bisA region in both cases. Such difference originates from the large difference in the thermal conductivity between α-alumina and bisA. Particularly in the M1n3 case, the temperature-gap ΔT at the interface is substantial. In both cases, there exist obvious changes at $z = 60 − 70$ Å in the temperature lowering behavior as z is increased. We consider that the changes are reflections of the artificial temperature control in the bisA region at $z = 70 − 85$ Å. The temperature profile is therefore physically reliable in the range $z = 10 − 50$ Å only.

To calculate the thermal conductivity, $\lambda = Jl/(T_1 − T_2)$ in Eq. (3.1), of the system, we choose a z-position of high temperature (T_1) at $z = 0$ Å in the α-alumina region and that of low temperature (T_2) at $z = 80$ Å in the bisA region; that is, $l = 80$ Å. Since the temperature profiles in Fig. 3.4 (top) are reliable only in the range of $z = 10 − 50$ Å, we evaluate T_1 and T_2 as follows. Due to the flatness of temperatures in the α-alumina region seen in Fig. 3.4 (top). We can assume $T_1 = 430$ K. As for T_2, we firstly obtain the least-squared fitted line of the data points in the range $z = 35 − 50$ Å and secondary extrapolate the line to $z = 80$ Å. Table 3.1 compares thereby calculated values of J, ΔT, $J/\Delta T$, and λ in all the cases. The J is obtained as

the average of input and output fluxes of heat; the relative difference between the two is less than 5% in all the cases.

The λ and $J/\Delta T$ in Table 3.1 enlarge by increasing either lengths (n) or number of the SC molecules, which suggests that a substantial proportion of heat flows through the SC molecules. We note that ΔT is quite sensitive to the setting of the SC molecules, while the flux J is insensitive to that. In the M32n3 case, ΔT is as small as 1.9 K. It is because thermal resistance of the interface is small due to large number (32) of the SC molecules. In fact, $J/\Delta T$ in the M32n3 case is 6.8 times as high as that in the M1n3 case. However, as the contribution of the bisA region to the effective thermal resistance is dominant, λ in the M32n3 case is only 1.4 times as large as that in the M1n3 case. Figure 3.5 shows such a relations between λ and $J/\Delta T$. The λ appears to be saturated for large $J/\Delta T$, the estimated saturation-limit value of $0.185\,\mathrm{W/m \cdot K}$ compares well with the theoretical value calculated using the present thermal conductivity $0.12\,\mathrm{W/m \cdot K}$ of bulk bisA multiplied by the inverse of the z-width proportion ($52/80 = 0.65$) of the bisA region in the system.
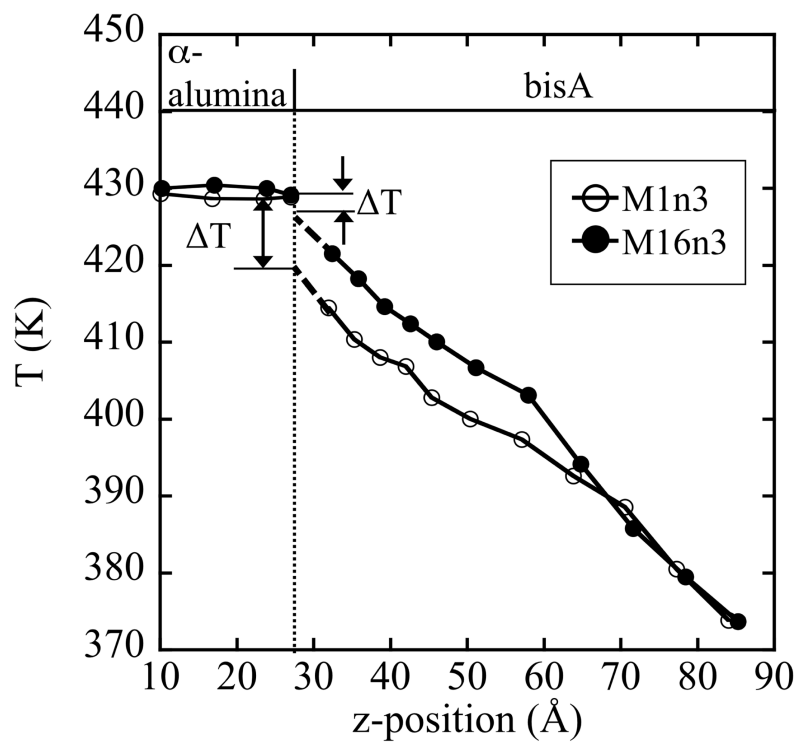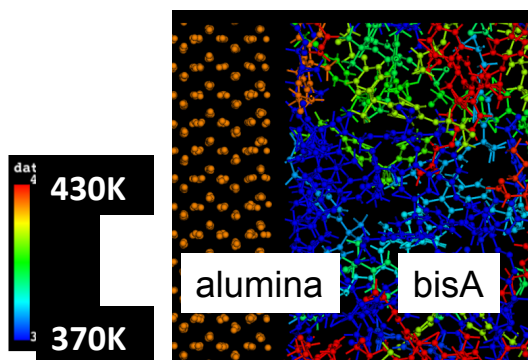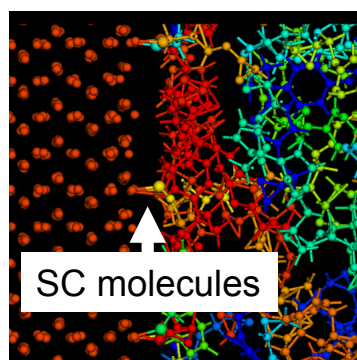
Figure 3.4: (top) Temperature profiles in the M1n3 and M16n3 cases. (bottom) The snapshots of atomic temperatures at the interface. (a) Case of M1n3. (b) Case of M16n3.
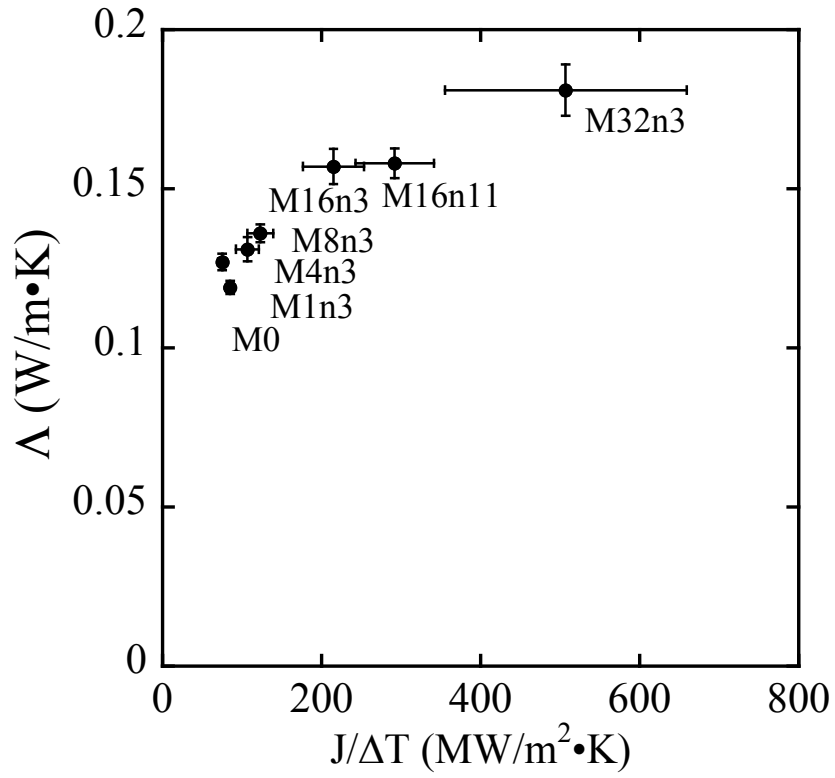
Figure 3.5: Relation between λ and $J/\Delta T$ in the present runs. Possible errors estimated are also drawn.

TABLE 3.1: The J, ΔT, $J/\Delta T$, and λ obtained in various cases of the present simulation.

case	number of SC molecules	n of $(CH_2)_n$	J (W/m^2)	ΔT (K)	$J/\Delta T$ (W/m$^2 \cdot$ K)	λ (W/m $\cdot$ K)
M0	0	$-$	8.17×10^8	9.6	8.51×10^7	0.119
M1n3	1	3	8.10×10^8	10.8	7.50×10^7	0.127
M4n3	4	3	8.68×10^8	8.1	1.07×10^8	0.131
M8n3	8	3	9.12×10^8	7.4	1.23×10^8	0.136
M16n3	16	3	9.25×10^8	4.3	2.15×10^8	0.157
M16n11	16	11	1.02×10^9	3.5	2.92×10^8	0.158
M32n3	32	3	9.63×10^8	1.9	5.07×10^8	0.181

3.2.2 Heat-transfer routes through interface

We investigate heat transfer routes from the α-alumina (i.e., filler) to bisA molecules (i.e., polymers) when the SC molecules are added in between. As stated above, a substantial proportion of heat flows from the α-alumina to SC molecules. It is because the SC molecules bond tightly to the α-alumina surface. We therefore consider the heat-transfer routes from the SC to bisA molecules by calculating the atomic temperature, defined as the time-averaged kinetic energy of a single atom in energy unit, for each atom around the SC molecules. We assume [28] that the difference in the atomic temperatures of a pair of atoms gets larger as the degree of thermal resistance between the two atoms becomes larger. With the assumption we compare the atomic temperatures of all atoms of the SC and neighboring bisA molecules to find the heat-transfer routes.

Figure 3.6(a) shows the atomic temperatures of the SC molecule and surface Al in the M8n3, M16n3, and M32n3 cases. The sequence in the horizontal axis corresponds to that in the SC molecule. The atomic temperatures in the M16n11 case (i.e., longer SC molecule) are shown in Fig. 3.6(b). Averages over the equivalent atoms of the SC molecules are performed in Fig. 3.6. As the error bars in Fig. 3.6 indicate, the atomic temperatures have accuracies of $0.5 - 1.5\,\text{K}$. We remind that the atomic temperatures agree among atoms (excluding H atoms) within $0.5 - 1.5\,\text{K}$ in an equilibrium run of a bulk bisA system at $T = 400\,\text{K}$.

We find in Fig. 3.6(a) that the atomic temperatures of the SC molecules in the M16n3 and M32n3 cases are much closer to that of the surface Al as compared to the M8n3 case. In the M16n3 and M32n3 cases, heat is therefore transferred more efficiently between the α-alumina and SC molecule and inside the SC molecule than between the SC and bisA molecules. Similar relatively efficient heat transfer inside the SC molecule is observed in the M16n11 case in Fig. 3.6(b). In the M8n3 case, on the other hand, heat transfer is more efficient between the SC and bisA molecules than between the α-alumina and SC molecule and inside the SC molecule. Since the bonding state of the Al-O pair between the α-alumina and SC

39

molecule and therefore its heat resistivity are essentially unchanged in all the cases, we conclude that heat flux from the SC to bisA molecules is impeded more in the M16n3, M32n3, and M16n11 cases than in the M8n3 case. Due to the large number of the SC molecule in the M32n3 case, however, such relatively high thermal impedance from the SC to bisA molecules contributes little to the overall thermal resistance.

We explain physical reasons of the relatively high thermal impedance between the SC and bisA molecules for both cases of large number (32) and long lengths ($n = 11$) of SC molecules. Figure 3.7 shows the numbers of bisA atoms in the 4.0 Å z-width bins prepared virtually from the α-alumina surface. The number approaches to the bulk value of around 85 in all the cases for $z > 15$ Å. By increasing either number of the SC molecules to 32 or length (n) of the SC molecule to 11, we find that the bisA atoms are pushed away significantly from the α-alumina surface. Since effective interaction between the SC and bisA molecules becomes weaker in the situation, heat transfer from the SC to bisA molecules is impeded. On the contrary, there exist substantial number of bisA atoms near the α-alumina surface in the M8n3 case. Those bisA atoms entangle the SC molecules, resulting in relatively efficient heat-transfer from the SC to bisA molecules.

We now consider the heat-transfer routes from the SC to bisA molecules from the difference or similarity of the atomic temperatures in the SC and neighboring bisA molecules. It is remarkable in the M8n3 case in Fig. 3.6(a) that the C-temperatures are substantially lower than the O-temperatures in the SC molecules. We remind that the inter-atomic interaction between the SC and bisA molecules is through the van der Waals and Coulomb forces. While the van der Waals forces are similar between various atomic pairs between the SC and bisA molecules, the Coulomb forces are significant between the C and O atoms of the SC and bisA molecules, respectively, because the charges are opposite in sign and the magnitude of O charge is large (see, Fig. 2.1(b)). We therefore conjecture that substantial proportion of heat is transferred from the C of the SC molecule to the O of bisA molecule through the Coulomb interaction when the SC molecules are surrounded by bisA molecules as in the M8n3 case.
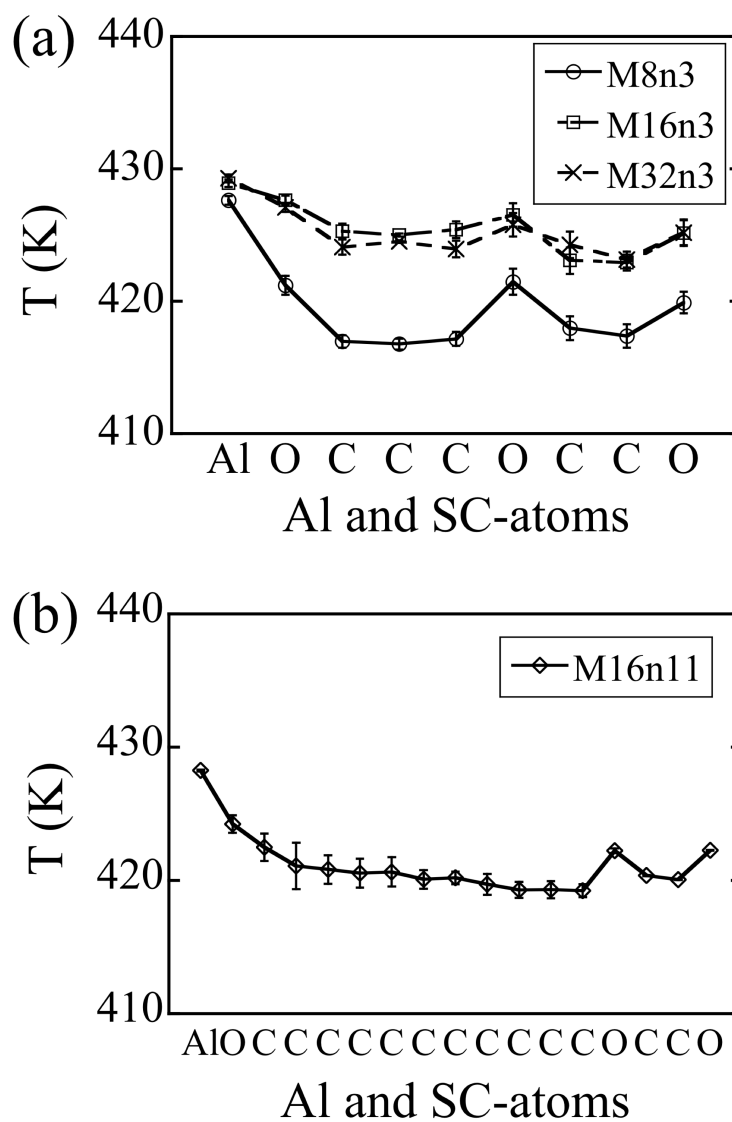
Figure 3.6: (a) Atomic temperatures of both surface Al atoms that bond to SC molecules and SC atoms in the M8n3, M16n3, and M32n3 cases. Possible errors estimated are also drawn. (b) Same as (a) but in the M16n11 case.

The conjecture mentioned above is supported by the atomic temperatures of bisA located within $5\,\text{Å}$ of the SC atoms depicted in Fig. 3.8. In Fig 3.8, we adopt the grouping rule of atoms used in the Dreiding inter-atomic potential: O atoms are divided into O1 (epoxy) and O2 (others); C atoms, into C2 (benzene) and C1 (others). The averaged atomic-temperatures of bisA in the M8n3 and M16n3 cases are higher than that in the M16n11 and M32n3 cases. It is much related to the increased effective interaction between the SC and bisA molecules in the M8n3 and M16n3 cases due to entanglement of the bisA to SC molecules as mentioned above. In the M16n3 case, the O1-temperature $(422\,\text{K})$ of the bisA is higher than other temperatures $(419-420\,\text{K})$ of the bisA and is close to the C-temperatures $(423-424\,\text{K})$ of the SC molecule. Similarly, the O1 and O2-temperatures $(420\,\text{K})$ of bisA are higher than other temperatures $(417-418\,\text{K})$ of bisA and correspond to the average of the C and O-temperatures of the SC molecule in the M8n3 case. We therefore conclude that a substantial proportion of heat is transferred from the C of the SC molecule to the O of neighboring bisA molecules when the density of the SC molecules on the interface is not large as in the M8n3. Since the atomic temperatures are homogeneous in the M16n11 and M32n3 cases, we guess that heat is transferred from the SC to bisA molecules through various atomic pairs when the density of the SC molecules on the interface is large or the lengths of the SC molecules are long.
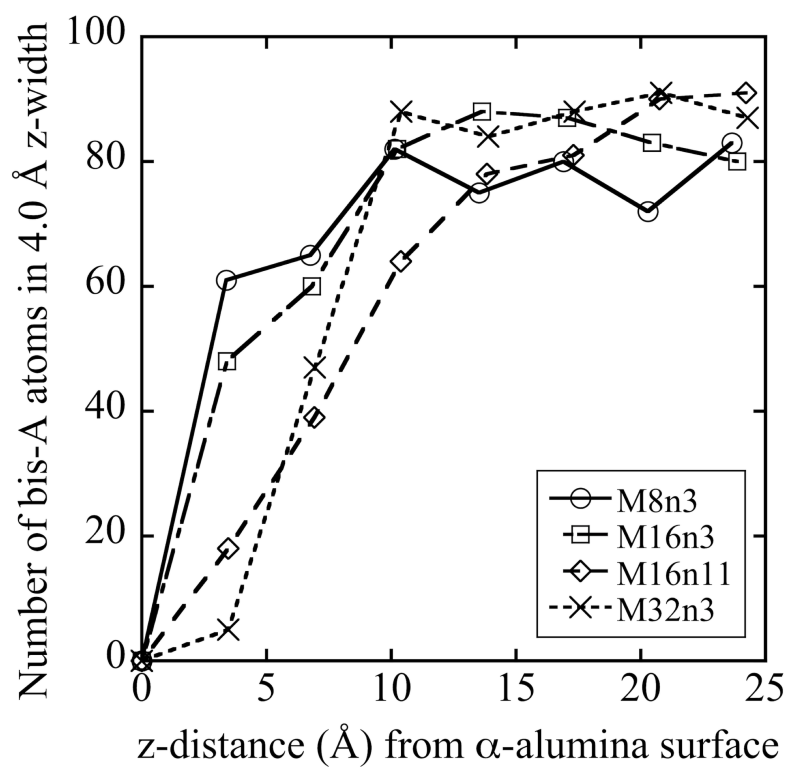
Figure 3.7: Numbers of bisA atoms in the 4.0 Å z-width bins prepared virtually from the α-alumina surface in the M8n3, M16n3, M16n11, and M32n3 cases.
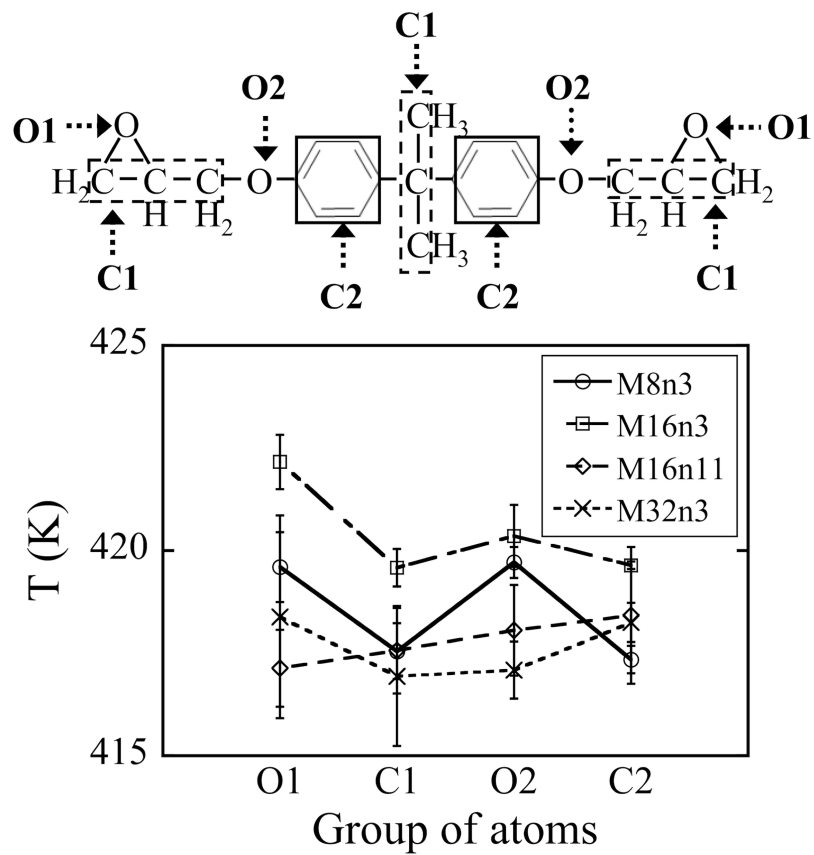
Figure 3.8: (top) Grouping of bisA atoms. (bottom) Atomic temperatures of the groups in M8n3, M16n3, M16n11, and M32n3 cases. Possible errors estimated are also drawn.

3.3 Conclusions

As for the situation of small packing fraction of fillers, we investigated the effects of the SC molecules on the interfacial thermal conductance by considering the interface system of thick polymers and filler [55]. The simulation system is considered composed of the bisphenol-A (bisA) epoxy region with 112 Å in z-width at the center and the α-alumina regions with (0001) surfaces to sandwich it. At the α-alumina -bisA interface, the model SC molecules have been inserted.

The NEMD simulation was performed for the system by changing number of SC molecules and their lengths. We have found that the thermal resistance at the α-alumina-bisA interface becomes smaller when either larger number of the SC molecules is added at the interface or their lengths are longer. The effective thermal conductivity of the system approaches to the value estimated by assuming zero thermal resistance at the interface. On the other hand, when the number of the SC molecules is small, thermal resistance between the SC to bisA molecules is small. In the situation, through detailed analyses of the polymer configurations and atomic temperature around the interface, a substantial proportion of heat is transferred from the C of the SC molecule to the O of neighboring bisA molecules.

Chapter 4

The situation of high packing fraction of fillers

To realize high thermal conductivity of the heat dissipation material, the packing fraction of the fillers is increased. When the packing fraction of the fillers is increased, the polymer region sandwiched by the fillers can be quite thin depending on the degree of filler agglomeration. The last chapter simulation results cannot be applied to such a situation because we have considered the interface of bulk bisA (as polymer) and α-alumina (as filler).

In this Chapter, we will consider the situation of a high packing fraction of α-alumina fillers with/without the SC molecules. We perform a series of the NEMD runs by changing the polymer depth and adding the SC molecules to understand their effects on the interfacial thermal conductance.

4.1 Setting in NEND

4.1.1 Simulation system for thermal conductivity

We consider the alumina-polymer-alumina system corresponding to the situation of high packing fraction of fillers in the composite for the NEMD simulation. Figure 4.1 (top) depicts a typical configuration of the system for the NEMD simulation. The two α-alumina slabs with Al termination are

placed on the left and right sides of the simulation box, while the polymer sub-system of depth D with or without the SC molecules are placed in between. The D is a distance between the surface layers of the two α-alumina slabs. The z-axis is set perpendicular to the interface as shown in Fig. 4.1. The periodic boundary conditions are applied for the x, y, and z-directions.

For the situation of a high packing fraction of α-alumina fillers, we replace the temperature control regions in the situation of small packing fraction of alumina fillers (Chap.3). The high and low temperature-controlled regions, at $T = 430$ and $370K$, are set in the α-alumina slabs to input and subtract the kinetic energies. The left (right) end of the left (right) α-alumina slab is fixed during a simulation run. To reduce long-range Coulomb interaction with the image slabs, two vacuum layers of 20 Å depth are set at both ends of the simulation box, and the dipole correction [56] is applied to the Ewald method.

Various values of the polymer depth, D, are considered. When the polymer sub-system contains no SC molecules, $L_z = 106$, 125, and 153 Å for $D = 14$, 33, and 61 Å, respectively. The L_x and L_y are fixed respectively to 34 Å and 38 Å, which are sufficiently longer that the chain length of a bisA molecule (~20 Å). The bisA molecules form an amorphous solid with nearly the same mass density of $0.86 - 0.88 \, \text{g/cm}^3$ in all cases. In the case of $D = 14$ Å, the system is composed of 8,660 atoms. We also consider the cases with the SC molecules inserted in the polymer sub-system. Total of 16 SC molecules are placed on the interface in a square lattice form (4×2) with their end atoms (O) bonded to surface Al's of two α-alumina surfaces. At the addition of the SC molecules we increase L_z from the original value to keep the mass density of the polymer sub-system to $0.86 - 0.89 \, \text{g/cm}^3$.

In the similar way as Chap. 3, for MD simulation, the velocity-Verlet algorithm is used to integrate the equations of atomic motion. The time step $dt = 1.0 \, \text{fs}$ is used and we omit H atoms in calculating the temperature profile. We confirm that the system is in the steady state after 1.5 ns by checking the difference between the input and subtracted energies per unit time in the temperature-controlled regions. The energy (heat) flux and
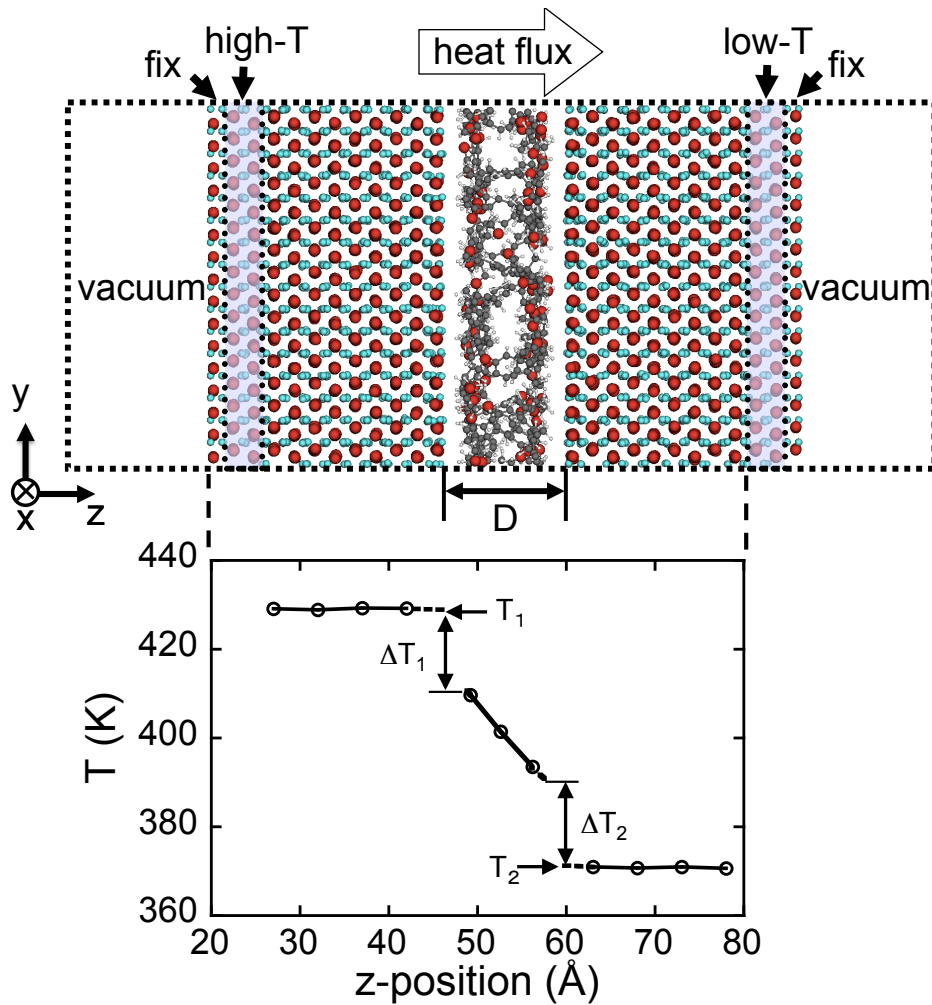
Figure 4.1: (top) Atomic configuration of a typical system for the NEMD simulation with D = 14Å without the SC molecules. Large red spheres are O's; medium cyan, Al's; medium grey, C's; small white, H's. (bottom) The temperature profile obtained in the NEMD run. Each point corresponds to the averaged kinetic energy of C, O, and Al-atoms in each 5.0Å z-widths.

temperature profile are obtained by averaging over 0.5 ns in the steady state.

Figure 4.1 (bottom) depicts the temperature profile for the case of $D = 14\,\text{Å}$ without the SC molecules. The temperature gradient is quite small in the α-alumina, while substantial in the bisA. The temperature-gaps ΔT_1 and ΔT_2 at the interfaces are significant. Majority of the thermal resistance of the polymer sub-system originates from such temperature gaps. The temperatures at the end z-positions of the α-alumina and bisA in close proximity to the interfaces are determined as follows. First, the end z-positions are defined as $z = 46\,\text{Å}$ for the α-alumina and $z = 48\,\text{Å}$ for the bisA for the left interface; $z = 58\,\text{Å}$ for the bisA and $z = 60\,\text{Å}$ for the α-alumina for the right interface. Since the end z-position of the bisA fluctuates in time and varies depending on the x-y location, we define it as the one separated by $2\,\text{Å}$ from the z-end (i.e., Al) of α-alumina. Then, the temperatures at those end z-positions are determined through linear extrapolation of data points (the open circles in Fig. 4.1 (bottom)).

4.2 Result and discussion

4.2.1 Thermal conductivity and interfacial thermal conductance

We calculate the effective thermal conductivity of the polymer sub-system by $\Lambda = JD/(T_1 - T_2)$ in Eq. (3.1). T_1 and T_2 are the high and low temperatures at the end z-positions of the α-alumina's at the interfaces. The effective thermal conductivity between two α-alumina's is a useful quantity to predict the effective thermal conductance of the whole composite material.

Figure 4.2 shows the D-dependence of Λ. We find in Fig. 4.2 that for both cases with and without the SC molecules, Λ decreases linearly as D decreases. Without the SC molecules, Λ for $D = 14\,\text{Å}$ is about 50 % of that for $D = 61\,\text{Å}$. With the SC molecules, Λ decreases by 20 % only when we change D from $67\,\text{Å}$ to $19\,\text{Å}$.

The Λ of the polymer sub-system is composed of the thermal conductivity

of the polymers and the interfacial thermal conductance. The thermal conductivity of the polymers is defined as

$$\lambda = J / \left(\frac{dT}{dz} \right),$$ (4.1)

where the temperature gradient $\frac{dT}{dz}$ is obtained at the central region of the polymers. The interfacial thermal conductance is defined as

$$J/\Delta T \quad \text{with} \quad \Delta T = (\Delta T_1 + \Delta T_2)/2,$$ (4.2)

where ΔT_1 and ΔT_2 are the temperature-gaps depicted in Fig. 4.1 (bottom). We note that the differences between ΔT_1 and ΔT_2 are smaller that 3 K in the present runs. Though the interfacial thermal conductance depends generally on the direction of heat flow [57,58], we cannot see substantial dependences. Figure 4.3 shows λ and $J/\Delta T$ for the cases without the SC molecules. In the case of $D = 14\,\text{Å}$ without the SC molecules, $\lambda = 0.10\,\text{W/m} \cdot \text{K}$ is close to that of the bulk bisA $(0.11 - 0.13\,\text{W/m}^2 \cdot \text{K})$ in Chap.3. On the other hand, $J/\Delta T$ for the case of $D = 14\,\text{Å}$ without the SC molecules is only about 50 % of that for the cases of $D = 33$ and $61\,\text{Å}$ without the SC molecules. We state that the significant linear-decrease in Λ for smaller D in Fig. 4.2 has resulted mainly from such a behavior in $J/\Delta T$.
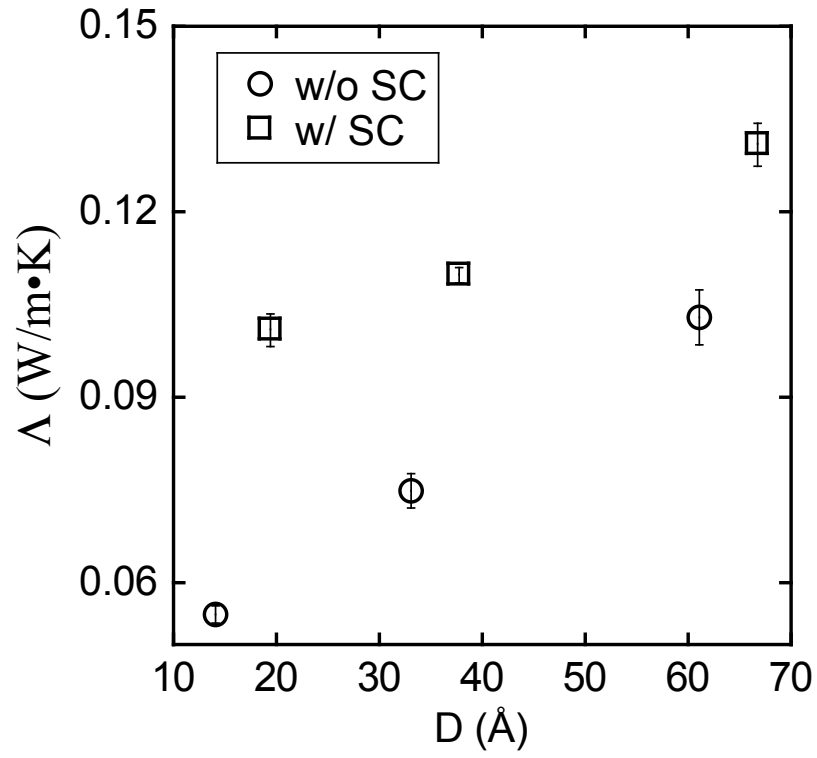
Figure 4.2: The effective thermal conductivities (Eq. 3.1) of the polymer sub-systems for various values of D with or without the SC molecules.
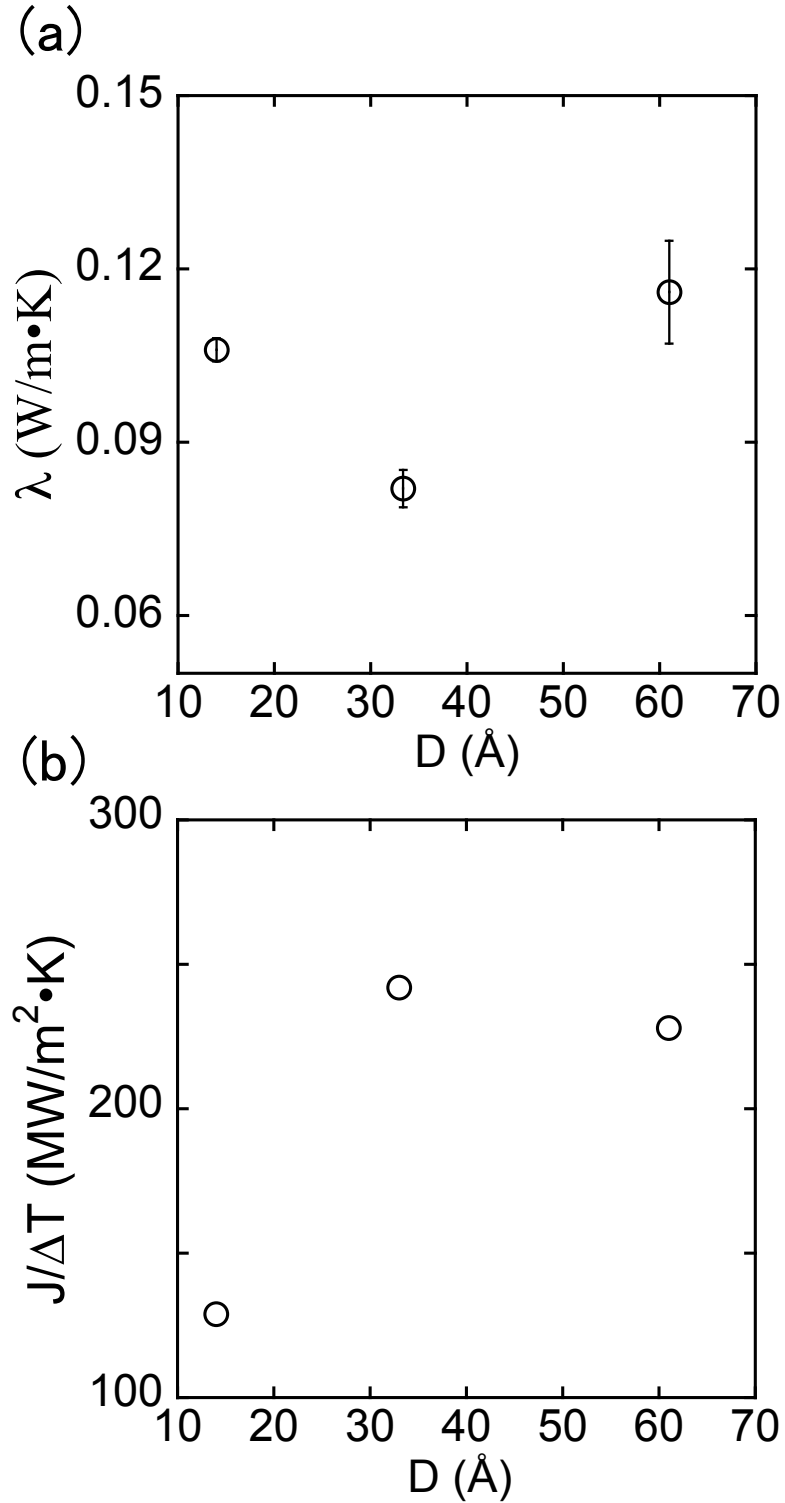
Figure. 4.3: (a) The thermal conductivities (Eq. 4.1) of the polymer sub-systems for various values of D without the SC molecules. (b) The interfacial thermal conductances (Eq. 4.2) for the same cases as (a).

We consider physical reasons of the relatively low interfacial thermal conductance, $J/\Delta T$, between the α-alumina and bisA in the case of $D = 14\,\text{Å}$ without the SC molecules. Figure 4.4 compares the numbers of the bisA atoms (C and O) in the 1.0 Å z-width bins prepared virtually from the α-alumina (left block) surface in the cases of $D = 14$ and $61\,\text{Å}$ without the SC molecules. In both cases, we observe accumulation of the bisA atoms near the α-alumina surface. It is a result of relatively strong Coulomb attraction between the surface Al of the α-alumina and O of the epoxy group in addition to between the O of the α-alumina and H of the bisA. It is noteworthy that the number of the bisA atoms within a few Å from the α-alumina surface is smaller in the $D = 14\,\text{Å}$ case than in the $D = 61\,\text{Å}$ case. It results from the structural stability of a bisA molecule. We find that the intra-molecular O-O distances between the two epoxy groups are $12.2 - 14.6\,\text{Å}$ in the $D = 14\,\text{Å}$ case and $12.1 - 14.9\,\text{Å}$ in the $D = 61\,\text{Å}$ case. Correspondingly the bending angles in overall V-shape of the bisA molecules are kept in the range of $110 - 124$ degrees. When D becomes close to the chain length ($\sim 20\,\text{Å}$) of a bisA molecule, substantial fraction of the bisA molecules are oriented to bridge between the two α-alumina slabs through attractive interaction of the O in the epoxy group and Al of α-alumina. In fact, we find that 11 out of 20 bisA molecules are in the bridging state. Such orientation constraint on the bisA molecules in the $D = 14\,\text{Å}$ case acts to lower the density of the bisA atoms at the interface as compared to the $D = 61\,\text{Å}$ case in which no such a constraint exists. The interfacial thermal conductance, $J/\Delta T$, gets smaller due to the weaker interaction at the interface resulting from lower density of the bisA atoms at the interface.

When the SC molecules are added to the system with $D = 14\,\text{Å}$, the effective thermal conductivity of the polymer sub-system, Λ, becomes 1.8 times as large as the original value. Addition of the SC molecules reduces deterioration of Λ of the polymer sub-system for smaller D. As depicted in Fig. 4.5, the SC molecules act to connect the polymers and α-alumina. Hence the interfacial thermal conductance, $J/\Delta T$, increases by about 20 %. Interestingly the thermal conductivity of the polymers, λ, also becomes 2.0 times as large as that for the case without the SC molecules. Such effects of
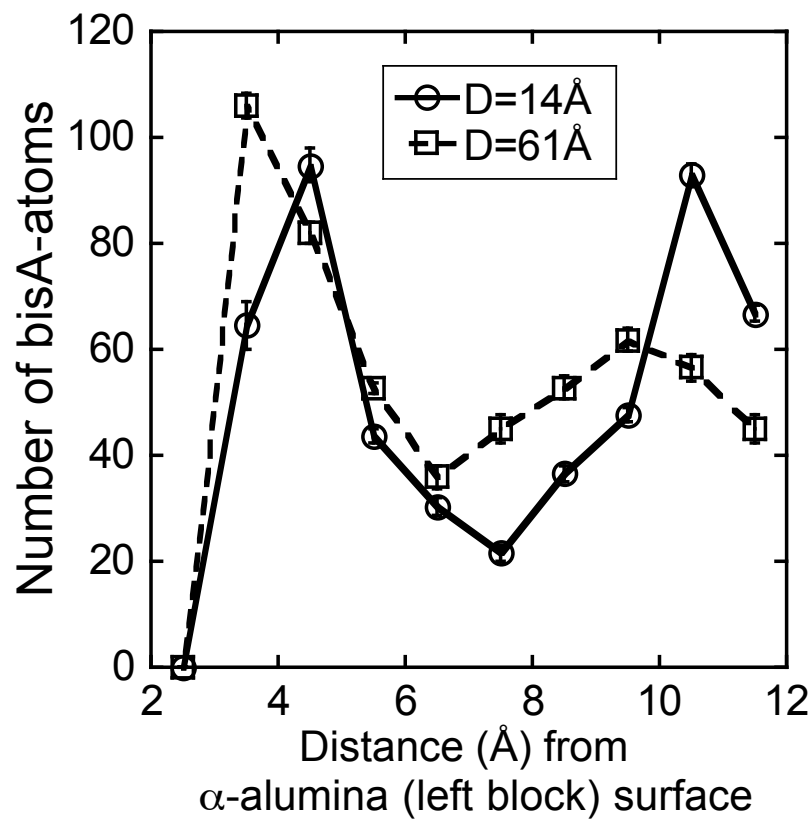
Figure 4.4: The numbers of C and O atoms of the bisA molecules in z-bins obtained through the NEMD simulation for the systems with $D = 14\,\text{Å}$ and $61\,\text{Å}$.
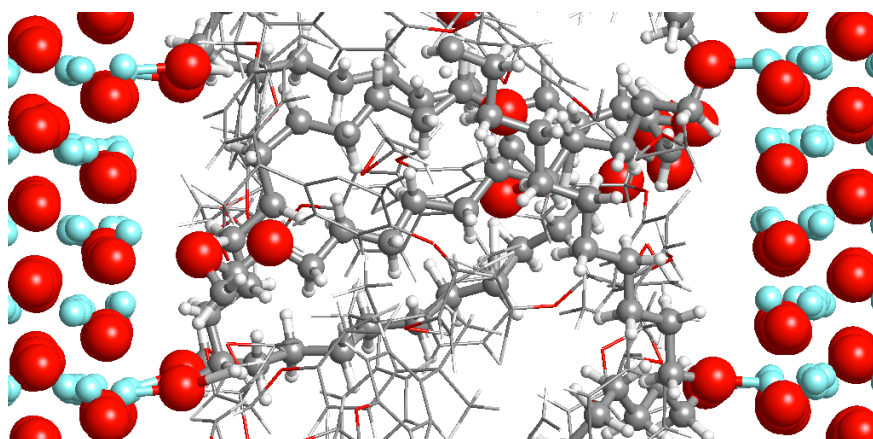
Figure 4.5: The close-up view of the simulation system for the case of $D = 14\,\text{Å}$ with the SC molecules. The SC molecules are drawn by spheres in the central region. The bisA molecules are drawn by sticks.

the SC molecules on the neighboring bisA molecules will be investigated in Chap. 5 through atomic vibration spectra analyses.

4.3 Conclusions

The overall thermal conductivity of the polymer-ceramic composite at a relatively high packing fraction of the ceramic fillers depends mainly on the effective thermal conductivities of the sandwiched polymer regions. Motivated by that we have performed the NEMD simulation to obtain the effective thermal conductivity of such a system, in which the bisA polymer sub-system with depth $14 - 70$ Å has been inserted between two α-alumina slabs. Effects of the SC agent have also been investigated by adding model molecules to the polymer sub-system. For smaller polymer-depth cases, the effective thermal conductivity is determined essentially by the interfacial thermal conductance relating to the temperature-gaps at the interfaces. Through the NEMD simulation, we have found for the interfacial thermal conductance that: (i) it is decreased by decreasing the polymer depth toward the chain length of a single bisA molecule, and (ii) it is increased by adding the SC molecule to the polymer sub-system.

Through detailed analyses of the polymer configurations, we have shown that the finding (i) has resulted from the decrease in the phonon transmission coefficient relating to effectively weakened interaction between a bisA molecule and two α-alumina slabs. The weakening has resulted because the orientation constraint on the bisA molecule due to attachment of each of the two epoxy groups to each of the two α-alumina slabs, lowers the density of the bisA atoms at the interface. Next chapter, we will explain reasons of the (ii) through combined analyses of atomic vibration spectra of the polymer sub-system and phonon wave-packet dynamics simulation.

Chapter 5

Heat transfer mechanisms

In Chap.4, through the NEMD, we found that interfacial thermal conductance is increased by adding the SC molecules to the polymer sub-system. Chapter 5 investigates these mechanisms related to the interfacial thermal conductance through atomic vibration spectra analyses and wave packet dynamics.

As shown in Chap.1.2, we remind that the heat flux J per unit area across the interface (normal to z-direction) from medium-a at temperature $T = T_a$ to medium-b at $T = T_b$ is expressed in Eq. (1.3).

$$
J = \frac{1}{V_a} \sum_{\text{mode},\vec{\eta}}^{+} v_{a,z}(\text{mode},\vec{\eta}) h f_a(\text{mode},\vec{\eta}) P_a(T_a,\text{mode},\vec{\eta}) t_{ab}(\text{mode},\vec{\eta})
$$

$$
+ \frac{1}{V_b} \sum_{\text{mode},\vec{\eta}}^{-} v_{b,z}(\text{mode},\vec{\eta}) h f_b(\text{mode},\vec{\eta}) P_b(T_b,\text{mode},\vec{\eta}) t_{ba}(\text{mode},\vec{\eta}) , \quad (1.3)
$$

with the volumes V's, phonon group velocities v's, phonon frequencies f's, phonon populations P's, and transmission coefficients t's. The summations are performed over the acoustic phonons, characterized with the wavelength vector $\vec{\eta}$ and transverse or longitudinal mode, in the first Brillouin zone with the direction of crossing the interface. It is assumed that the incident phonon keeps its frequency after crossing the interface. To clarify the situation, we here assume that medium-a is a hard crystalline material, e.g., α-alumina and that medium-b is a soft one, e.g, polymers. In the limit of

$T_a = T_b$, the partial flux from medium-a to b should cancel with the one from medium-b to a, from the principles of detailed balance. To have a higher interfacial thermal conductance, such partial fluxes need be larger.

As for the first term on the right hand side of Eq. (1.3) (i.e., the partial flux from medium-a to b), only t_{ab} can change by decreasing D or addition of the SC molecules due to the hardness of medium-a. On the other hand, all the terms in the second term on the right hand side of Eq. (1.3) (i.e., the partial flux from medium-b to a) can change. In this Chap. we suggest that addition of the SC molecules to the polymer sub-system in the present model enhances the phonon population (P_b) of medium-b in the acoustic frequency range of medium-a. Corresponding enhancement in t_{ab} as well as in $v_{b,z}$ will be studied in Chap. 5.2 through the wave-packet dynamics simulation.

5.1 Atomic vibration spectra analyses

We begin with evaluating the phonon population of bulk α-alumina at $T = 300$ K. The phonon population at frequency f for a given wavelength vector $\vec{\eta}$ is evaluated through the equilibrium MD simulation as

$$P_l(f,\vec{\eta}) = \left| \frac{1}{N n_s} \sum_{j=1}^{N} \sum_{n=0}^{n_s-1} \vec{v}_j(n\Delta t) \cdot \hat{\eta} \exp\left(i \frac{2\pi}{\eta} \vec{r}_j \cdot \hat{\eta} - i 2\pi f n \Delta t \right) \right|^2, \qquad (5.1)$$

$$P_t(f,\vec{\eta})$$
$$= \left| \frac{1}{N n_s} \sum_{j=1}^{N} \sum_{n=0}^{n_s-1} [\vec{v}_j(n\Delta t) - (\vec{v}_j(n\Delta t) \cdot \hat{\eta})\hat{\eta}] \exp\left(i \frac{2\pi}{\eta} \vec{r}_j \cdot \hat{\eta} - i 2\pi f n \Delta t \right) \right|^2, \qquad (5.2)$$

for longitudinal and transverse modes, respectively. There are always three acoustic modes: one longitudinal acoustic mode and two transverse acoustic modes. The phonon population follows the Bose-Einstein statistics with quantum statistical mechanics. However, in a classical MD simulation the phonon population should follow the Maxwell-Boltzmann statistics with statistical thermodynamics. The $f = f_m \equiv m/n_s\Delta t$ with natural number m, $\vec{\eta} = (L_x/n_x, L_y/n_y, L_z/n_z)$ with integer vector (n_x, n_y, n_z), $\hat{\eta} = \vec{\eta}/|\vec{\eta}|$, total number of atoms N, number of sampling points n_s, and time interval of

sampling Δt. To cover the frequency range $0 - 10$ THz of our interest, we set $n_s = 6,000$ and $\Delta t = 15$ fs. Because of limitation in the total sampling period $t_{total} \sim 90$ ps, f in Eqs. (5.1) and (5.2) may contain uncertainties of $\pi/t_{total} \sim 0.03$ THz. Therefore P_l (P_t) at a given f_m is obtained after averaging over ± 5 data points of m to reduce fluctuation. The system size of α-alumina is $(L_x, L_y, L_z) = (34.0\,\text{Å}, 38.0\,\text{Å}, 39.0\,\text{Å})$ with the periodic boundary conditions. We set the wavelength vector parallel to z-direction. We consider the cases of $\eta = 39.0$, 19.5, and $13.0\,\text{Å}$ by setting $n_z = 1, 2, \text{and } 3$, respectively, which correspond respectively to the wavenumbers $0.33(2\pi/a)$, $0.66(2\pi/a)$, and $2\pi/a$ with the lattice constant $a = 13.0\,\text{Å}$ of α-alumina in (0001)-direction. We set the time step $dt = 1.0$ fs in the MD simulation.

Figure 5.1 (a) shows the frequency dependencies of P_l and P_t for bulk α-alumina at $T = 300$ K at the three $\vec{\eta}$'s. At the longest wavelength of $\eta = 39.0\,\text{Å}$, P_l (P_t) has a strong and sharp peak at $f = 1.2$ (2.7) THz. At shorter wavelengths, such P-peaks spread in frequency, which means shorter life times. Figure 5.1 (b) shows relative intensities of the P-peaks, which appear to follow the Maxwell-Boltzmann statistics of the phonon energy as expected. To plot Fig. 5.1 (b), intensity of a P-peak is calculated by integrating the population around the central frequency (see Fig 5.1 (a)). The phonon dispersion relation evaluated from Fig. 5.1 (b) compares well with the one calculated with the DFT calculation as shown Fig 5.2. The longitudinal phonon frequency ranges in $0 - 10$ THz, while the transverse one in $0 - 5$ THz.

We now consider the phonon population for the bisA. First we set a single bisA molecule only in a simulation box of $(L_x, L_y, L_z) = (34.0\,\text{Å}, 38.0\,\text{Å}, 39.0\,\text{Å})$ with a connecting vector between the two epoxy O's parallel to z-direction; orientation of the vector is kept during the MD run. The average $(2P_t + P_l)/3$ for $\eta = 13.0\,\text{Å}$ $(n_z = 3)$ for the case of a single bisA molecule at $T = 100$ K is depicted in the inset of Fig. 5.3; H atoms are omitted in P_l and P_t. In the range of $0 - 8$ THz, as expected, we observe several sharp peaks corresponding to the molecular vibration modes. In the lowest mode of $f = 0.8$ THz, the molecule vibrates as the two epoxy groups flap like a butterfly wings. If the temperature is increases to $T = 300$ K, those peaks decompose
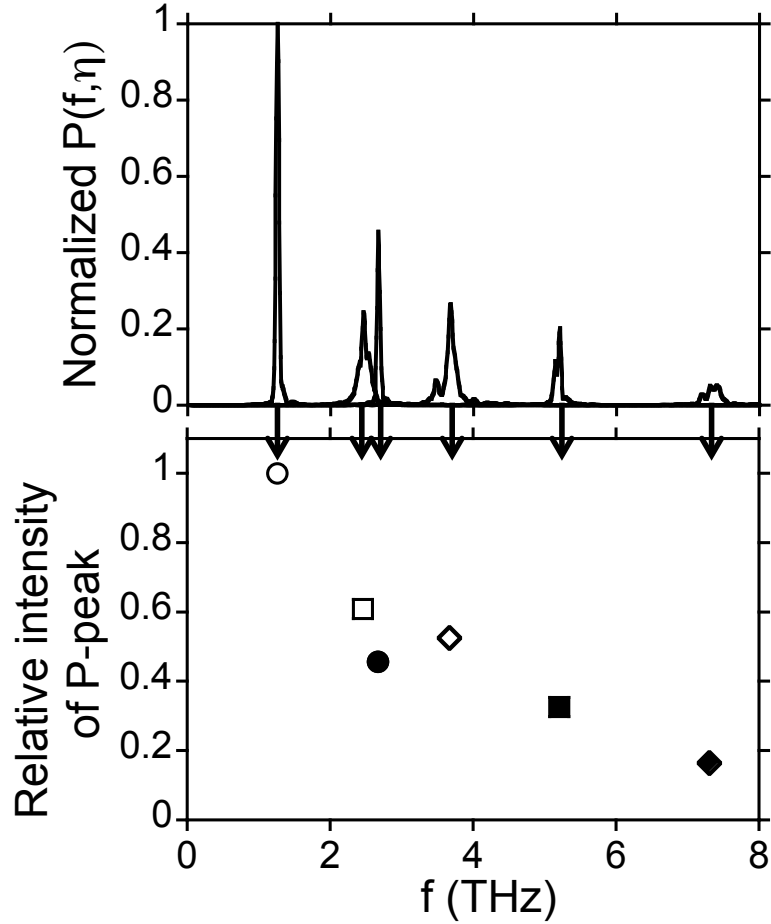
Figure 5.1 (a) The P_l and P_t (Eqs. 5.1 and 5.2) of bulk α-alumina at $T = 300$ K for three $\vec{\eta}$'s parallel to z-direction, normalized by the largest value at $f = 1.2$ THz. (b) Relative intensities of the peaks in (a). The open symbols are for P_t; closed ones, for P_l.

to many peaks with substantial broadening. It is a reflection of increased degrees of non-linearity in the inter-atomic potential at a higher temperature. Second we prepare bulk bisA with the same simulation box size. Figure 5.3 shows the average $(2P_t + P_l)/3$ for $\eta = 13.0$ Å $(n_z = 3)$ for the bulk bisA at $T = 300$ K obtained through three MD runs for 120 ps. Significant broadening in Fig. 5.3 in comparison to Fig. 5.3 (inset) means that the phonon picture in the wavenumber space may be inappropriate in
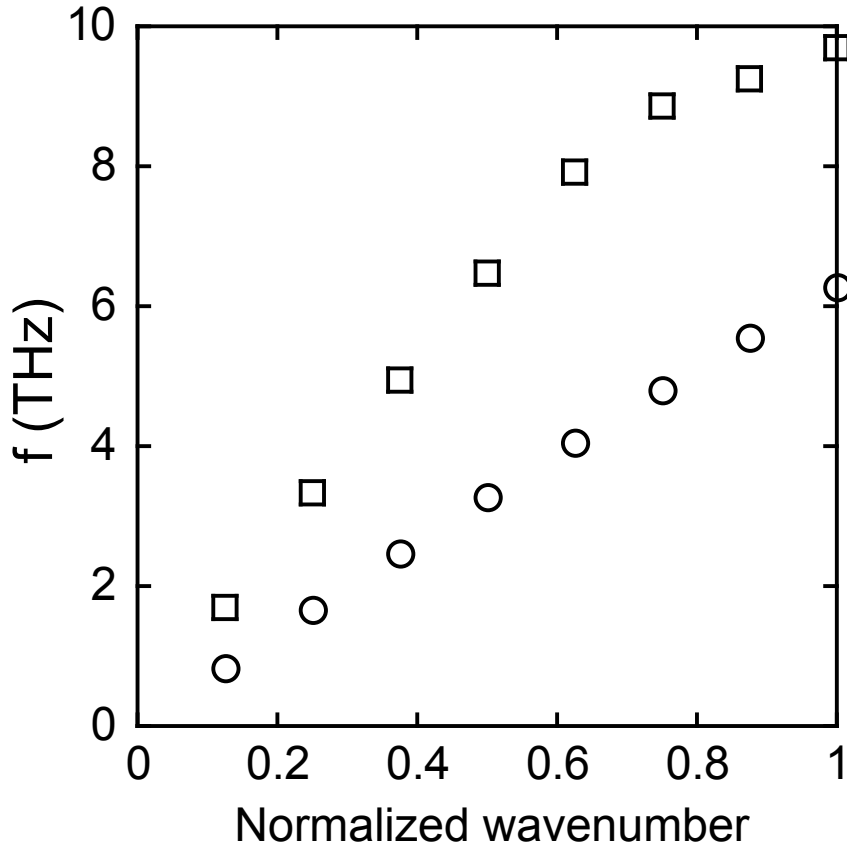
Figure 5.2: The phonon dispersion relation with DFT calculation. The longitudinal phonon frequency ranges in $0-10$ THz, while the transverse one in $0-5$ THz.

the case because of the non-linearity in the inter-atomic potential and the randomness in the molecular configurations.

We therefore integrate over the wavenumbers (inverse of $\vec{\eta}$) in Eqs. (5.1) and (5.2) before summation over the atoms for better statistics in analyzing possible changes in the phonon or vibrational-mode population by addition of the SC molecules, which reduces to the vibration spectrum of each atom. It is useful for the purpose to group atoms following the grouping rule used in the Dreiding inter-atomic potential. We therefore calculate
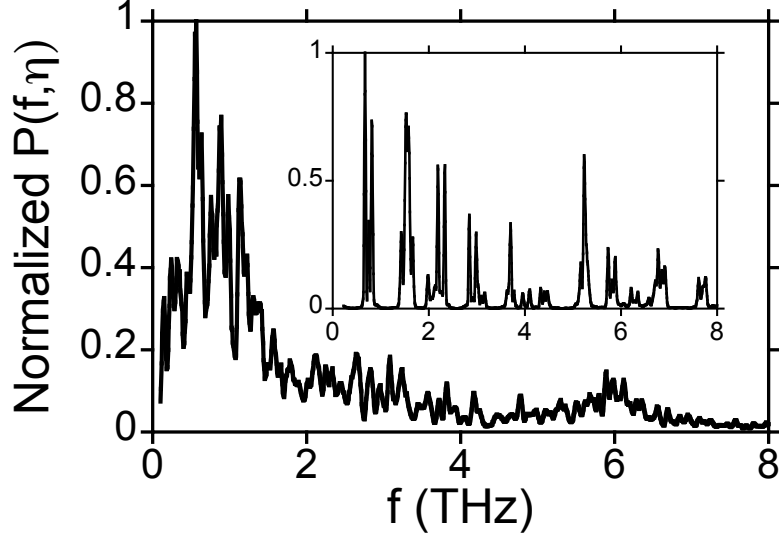
Figure 5.3: The average $(2P_t + P_l)/3$ of bulk bisA at $T = 300\,\text{K}$ for $\vec{\eta} = (0,0,13.0\text{Å})$. The inset corresponds to the case of a single bisA molecule at $T = 100\,\text{K}$ for the same $\vec{\eta}$.

$$P_{\text{group}}(f) = \frac{1}{N_g} \sum_{j=1}^{N_g} \left| \frac{1}{n_s} \sum_{n=0}^{n_s-1} \vec{v}_j\,(n\Delta t)\,\exp(i2\pi f n\Delta t) \right|^2 \tag{5.3}$$

for a given group. The groups for the bisA are the following: O atoms are grouped into O1 (epoxy) and O2 (others), C into C2 (benzene) and C1 (others) as depicted in Fig. 5.4 (a). As for the SC, O into O3 (bonded to Al), O5 (epoxy) and O4 (other), and C into C3. The N_g in Eq. (5.3) is the number of atoms in a group. We consider $f = 0.30,\ 3.0$ and 6.0 THz. We note that $f = 3.0$ and 6.0 THz corresponds to typical phonons of α-alumina: $f = 0.3$ to the lowest mode of the bulk bisA in Fig.5.3. In the bulk bisA case, peak of phonon population are broadening, $f = 0.3$ THz contains vibrations of winds (i.e., epoxy groups) of bisA molecules.

Figure 5.4 (b) shows P_{group}'s for the bulk bisA at $T = 300\,\text{K}$, normalized by the value for O1-group at $f = 3.0$ THz. The P_{group} for O1-group assumes the largest value at $f = 3.0$ THz. This relatively fast vibration at $f = 3.0$ THz is caused by the Coulomb interaction between O1 (charge, $-0.371\,e^-$) and C1

$(0.105\ e^-)$ of surrounding molecules. If we make N_g-weighted average of P_group, that is, simple sum of the absolute squares in Eq. (5.3) over all the atoms, we find that the population at $f = 0.30$ THz is the largest. Figure 5.4 (c) shows P_group's in the polymer sub-system for the case of $D = 14\,\text{Å}$ without the SC molecules at equilibrium $T = 300\,\text{K}$, normalized by the same value used in Fig. 5.4 (b). As seen in Fig. 5.4 (c), P_group's at $f = 0.30$ THz are substantially smaller than that for the bulk bisA. As stated in the last section, a bisA molecule in the case of $D = 14\,\text{Å}$ without the SC molecules is effectively constrained by the two α-alumina's. Those constrained bisA molecules cannot oscillate freely at $f = 0.30$ THz in the butterfly-like mode. We note that such a change at $f = 0.3$ THz does not affect substantially the interfacial thermal conductance because the phonon population at such a low frequency is small for α-alumina. The P_group for O1-group at $f = 3.0$ THz in Fig. 5.4 (c) is significantly larger that that of the bulk bisA in Fig. 5.4 (b), while that of the other group (O2) changes little. The change comes from those O1 atoms interacting much with the surface Al's of α-alumina. Though $f = 3.0$ THz corresponds to middle of the acoustic phonon frequency range of α-alumina, the change in P_group for O1-group only has little effect on the thermal conductivity of the polymers, as demonstrated in the last section through the NEMD results. The decrease in the interfacial thermal conductance for the case of $D = 14\,\text{Å}$ without the SC molecules should have resulted from decreased transmission coefficients (t_{ab} and t_{ba}) due to decreased local atomic density of the polymers at the interface (see Fig. 4.4).

The P_group's for the case of $D = 14\,\text{Å}$ with the SC molecules are shown for the bisA molecules in Fig. 5.4 (e) and for the SC in Fig. 5.4 (d); both are normalized by the same value used for Fig. 5.4 (b). As seen in Fig. 5.4 (e), P_group's for the O1, C1, and C2-groups of the bisA increase significantly at $f = 3.0$ THz by the influence of the SC molecules (see Fig. 5.4 (d)). We guess that addition of the SC molecules enhances the phonon population of the bisA in the acoustic phonon frequency range of α-alumina by making the bisA effectively stiffer through entanglement of the bisA and SC molecules.
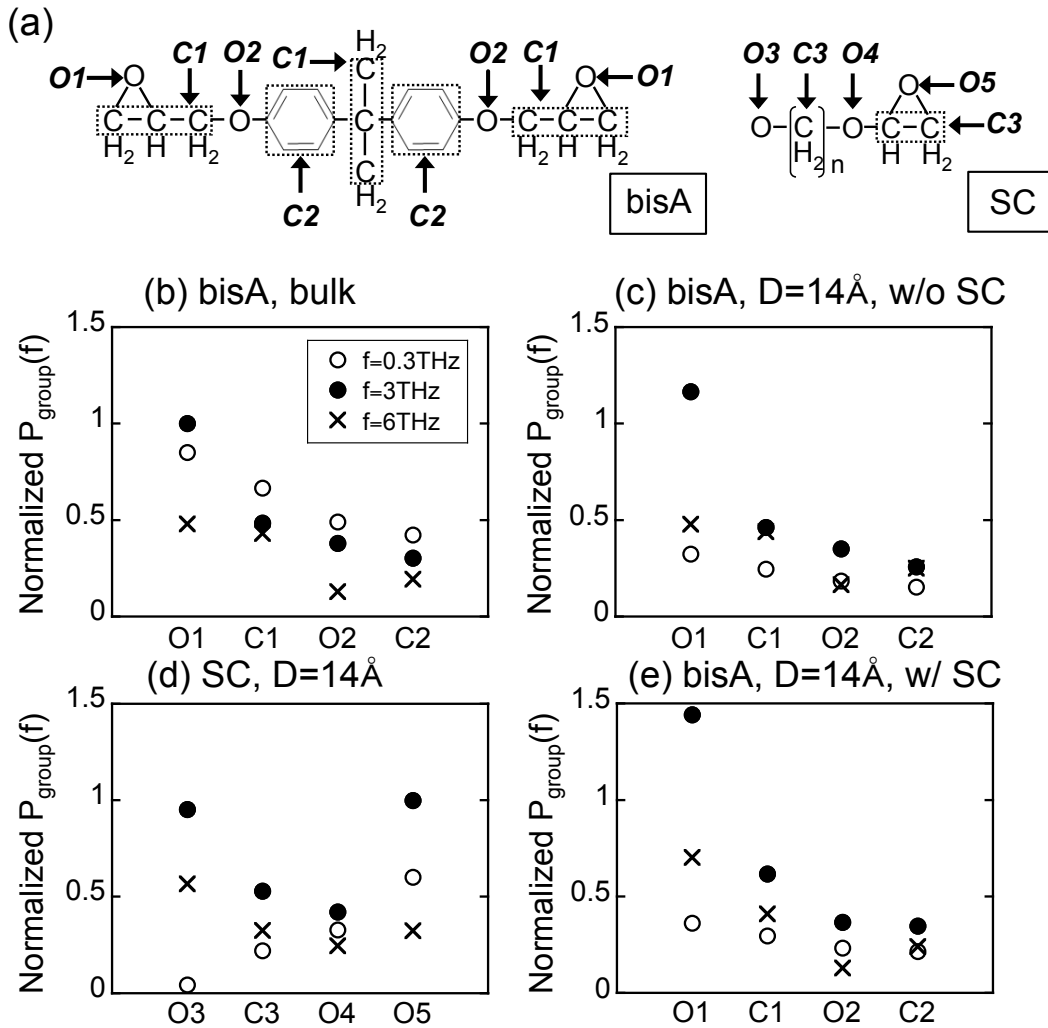
Figure 5.4: (a) The grouping of C and O atoms. (b) The P_{group} of bulk bisA at $T = 300\,\mathrm{K}$. (c) The P_{group} of the bisA for the case of $D = 14\,\text{Å}$ without the SC at $T = 300\,\mathrm{K}$. (d) The P_{group} of the SC for the case of $D = 14\,\text{Å}$ with the SC at $T = 300\,\mathrm{K}$. (e) The P_{group} of the bisA for the case of $D = 14\,\text{Å}$ with the SC at $T = 300\,\mathrm{K}$.

5.2 Phonon wave packet dynamics

The interfacial thermal conductance is related to the phonon transmission coefficient and group velocity. The NEMD simulation cannot give such detailed information of the heat transfer. Chapter 5.2 investigates those issues through the phonon wave-packet dynamics simulation.

In the simulation, we initially set an acoustic phonon wave-packet by controlling atomic positions and then perform an MD run to trace the time evolution of the wave packet. We control potential energies of those atoms at the displacement-controlled area to obtain wave packet. In a similar way to the NEMD, we assume thermal equilibrium at an area away from the displacement-controlled one. We thereby obtain the transmission coefficient through the interface for the wave packet characterized by the wavelength and mode (transverse or longitudinal). Figure 5.5 depicts a typical configuration of the system in the present phonon wave-packet dynamics simulation. We replace the left α-alumina slab used in the NEMD simulation by a thick slab of depth 130 Å to set a wave packet. We consider the D-dependence of the wave-packet transmission. The system sizes are $(L_x, L_y, L_z) = (34\text{Å}, 38\text{Å}, 210\text{Å})$ and $(34\text{Å}, 38\text{Å}, 229\text{Å})$ for the cases of $D = 14$ and 33 Å without the SC molecules, respectively. In addition, we consider the cases with 16 SC molecules to analyze their effects on the transmission; as in the NEMD simulation, L_z is increased from the original value to keep the mass density of the polymer sub-system to $0.86 - 0.89\,\text{g/cm}^3$. To suppress artificial reflection of the wave packet at the ends of the α-alumina slabs, we set damper regions; the damper width is 26.5 Å (5.3 Å) for the left (right) α-alumina slab, as shown in Fig. 5.5 (top).

Among acoustic and optical phonons in α-alumina, we consider that the heat transfers mostly through the acoustic phonons due to their large group velocities. To set initially the acoustic wave-packet in the left α-alumina slab, we obtain the minimum energy configuration of atoms under the condition that the averaged displacement R_{iz} of those atoms contained in i-th z-width of 2.17 Å, which corresponds to one sixth of c-axis length (13.0 Å) of the α-alumina unit-cell, is
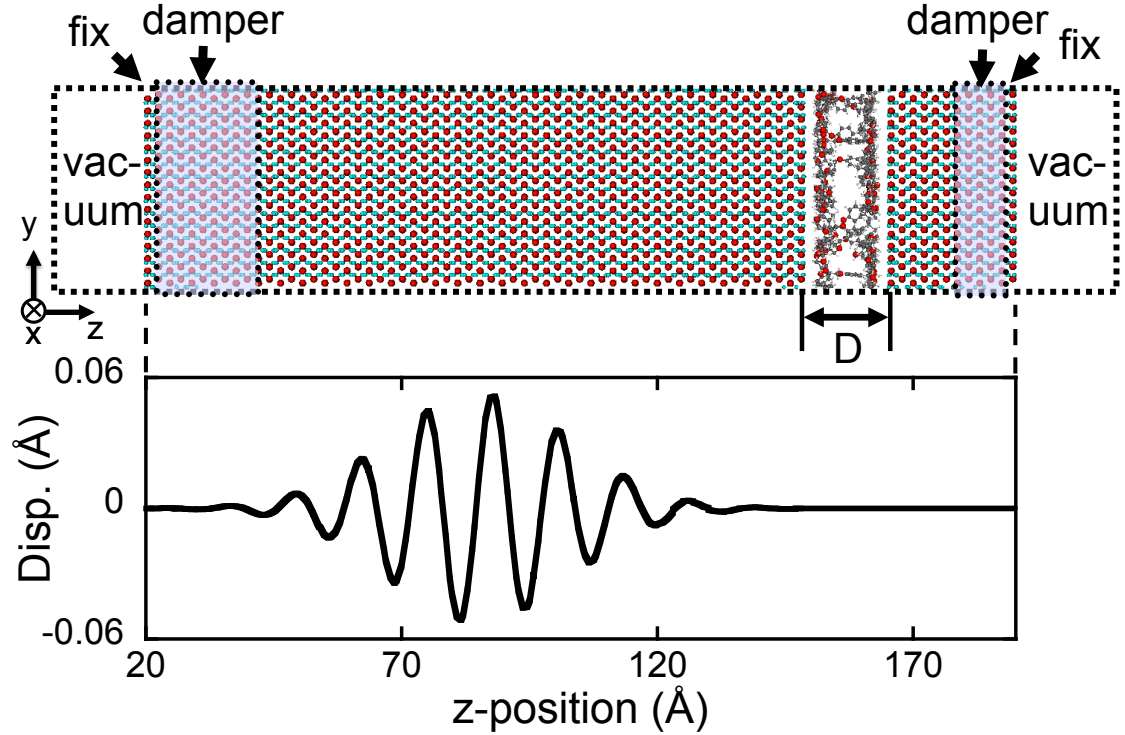
Figure 5.5. (top) Atomic configuration of the system in the case of $D = 14\,\text{Å}$ without the SC molecules for the wave-packet dynamics simulation. (bottom) The displacement profile applied to the system in (top).

$$A \sin \frac{2\pi R_{iz}}{\eta} \exp\left(-\frac{(R_{iz} - R_0)^2}{2\sigma^2}\right), \qquad (5.4)$$

with $A = 0.053\,\text{Å}$, $\sigma = 18\,\text{Å}$, and the central z-position R_0 of the wave packet.

For high numerical accuracy, we apply small constant forces, which are the reverse of the residual atomic force vectors at the initial configuration, to the atoms in the polymer sub-system. The displacements are parallel to z-direction for the longitudinal mode, while y-direction for the transverse mode. We consider three wavelengths $\eta = 13.0$, 26.0, and 39.0 Å. By performing the MD simulation we monitor the time evolutions of the spatial distributions of the kinetic and potential energies. Both are found to show the same behavior. Since the wave-packet dissipates significantly in the
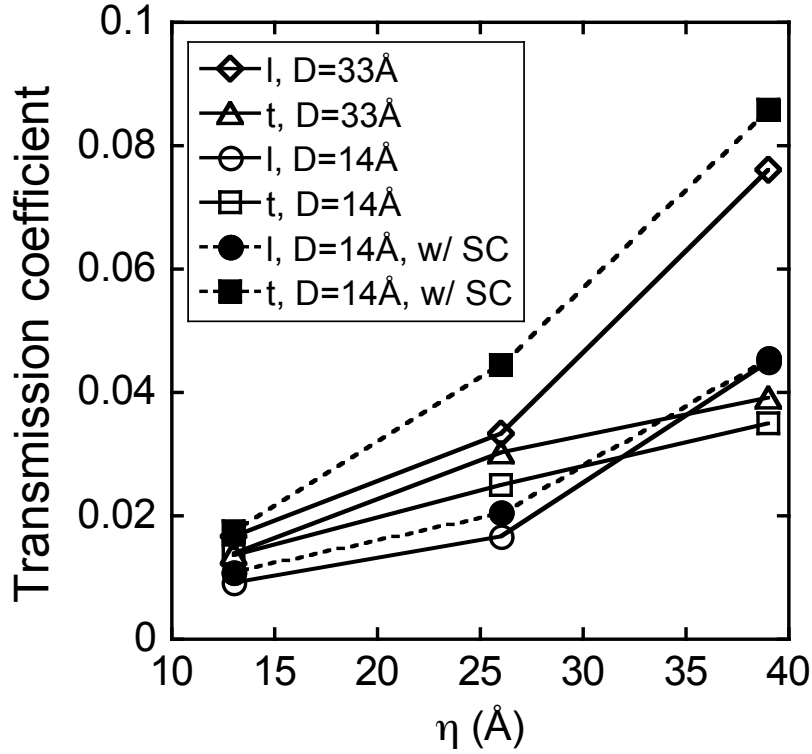
Figure 5.6: The transmission coefficients of longitudinal (l) and transverse (t) wave-packets obtained through the wave-packet dynamics simulation for $D = 14$ and 33 Å with or without the SC molecules.

polymer sub-system, we focus on analyzing the wave-packet transmission from the α-alumina slab to the polymer sub-system.

Figure 5.6 shows the transmission coefficients for various combination cases of the wavelength η, mode (longitudinal or transverse), and with or without SC molecules. Here the transmission coefficient is defined as the ratio in total (i.e., kinetic plus potential) energy increment between the transmitted wave-packet in the polymer sub-system to the incident one in the α-alumina slab. In general the transmission coefficient is larger for larger η because it has a smaller frequency and hence can transform to a phonon with the same frequency that exists in the soft polymer. In the following we therefore concentrate on comparing the cases with $\eta = 39.0$ Å to analyze three kinds of effects (D, mode, and SC molecules) on the transmission coefficient.

First we analyze the effects of the polymer sub-system depth, D, on the transmission coefficient. Since the longitudinal wave involves change in local pressure, surface of the polymer sub-system is forced to move. Accurate determination of the transmission coefficient therefore requires waiting about 1 ps until the possible wave reflection occurs. We thereby find for the longitudinal mode with $\eta = 39.0$ Å that the transmission coefficient is 0.045 for the case of $D = 14$ Å without the SC molecules, while 0.076 for case of $D = 33$ Å without the SC molecules. The significant decrease in the transmission coefficient of longitudinal mode for smaller D is related to the decrease in the interfacial thermal conductance found for smaller D in the NEMD simulation. For the transverse mode, on the other hand, the transmission coefficient changes little.

Second we analyze further the effects of mode on the transmission coefficient. Significant difference in the transmission coefficient between the transverse and longitudinal waves with $\eta = 39.0$ Å is seen in Fig. 5.6. The transmission coefficients for the cases of $D = 14$ and 33 Å without the SC molecules is higher for the longitudinal mode than for the transverse mode. To investigate further the mechanisms of the difference, we depict in Fig. 5.7 the time evolution of the displacement of the transmitted wave with $\eta = 39.0$ Å in the polymer sub-system for the cases of $D = 14$ Å with and without the SC molecules (D is slightly larger than 14 Å after addition of the SC molecules). In each panel of Fig. 5.7, the solid and dashed curves correspond respectively to the left and right end-regions (5 Å width) in the polymer sub-system. The displacements are normalized by A in Eq. (5.4). Figures 5.7 (a) and 5.7 (c) show the results for the case without the SC molecules for the longitudinal and transverse modes, respectively. For the longitudinal mode, the maximum displacement in the left end-region of the polymer sub-system is the same as the one of the α-alumina due to the volume change nature of the mode. However displacement of the right end-region becomes quite small, which means that the longitudinal mode dissipates quickly in the polymer sub-system. For the transverse mode, the maximum displacement in the polymer sub-system is 0.16 as seen in Fig. 5.7 (c), which is much smaller than in the longitudinal mode. However,
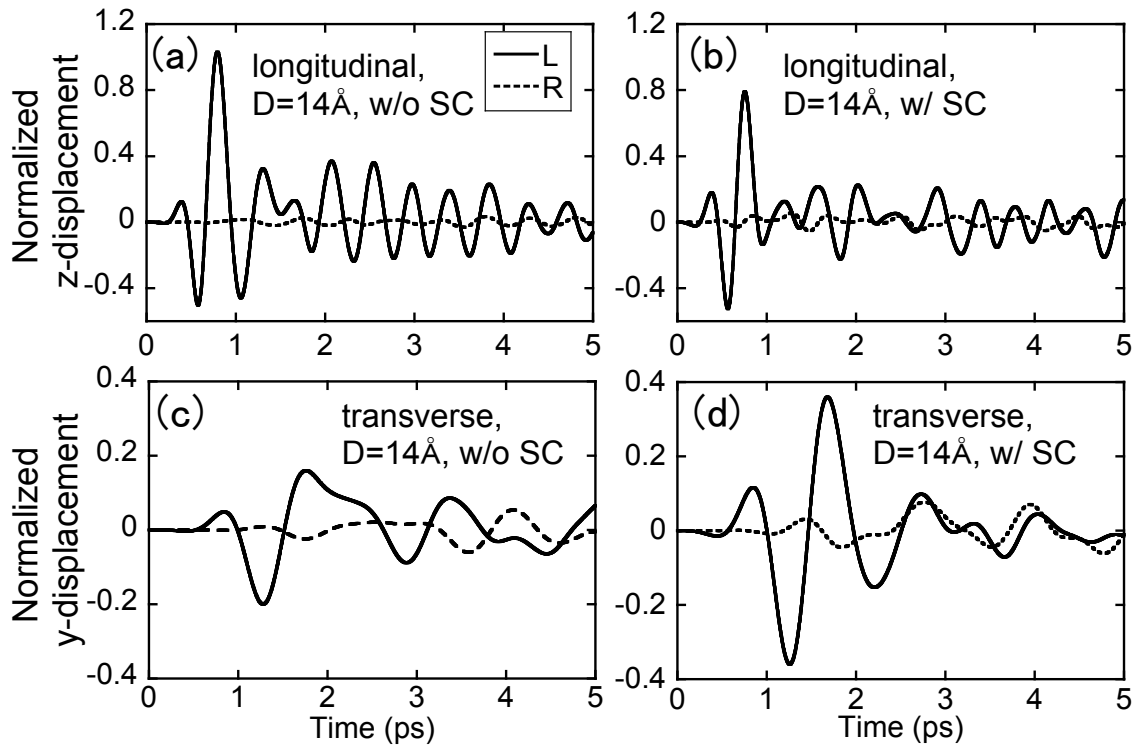
Figure 5.7. The time evolutions of z and y-displacements at the left (L) and right (R) end-regions of the polymer sub-system in various cases of the wave-packet dynamics simulation: (a) for longitudinal mode in the case of $D = 14\,\text{Å}$ without the SC; (b) for longitudinal mode in the case of $D = 14\,\text{Å}$ with the SC; (c) for transverse mode in the case of $D = 14\,\text{Å}$ without the SC; (d) for transverse mode in the case of $D = 14\,\text{Å}$ with the SC.

displacement of the right end-region is the same order as that of the left end-region with the phase shifted significantly, which is a reflection of relatively slow group velocity of the wave in the polymer sub-system.

Third we analyze the effects of SC molecules on the transmission coefficient. Figures 5.7 (b) and 5.7 (d) depict the displacements of the polymer sub-system in the case of $D = 14\,\text{Å}$ with the SC molecules for the wave packet with $\eta = 39.0\,\text{Å}$ in the longitudinal and transverse modes, respectively. For the longitudinal mode, addition of the SC molecules does not change the transmission coefficient substantially (see Fig. 5.6). We find in Fig. 5.7 (b) that the displacement in the right end-region is similar to the case without the SC molecules for the longitudinal mode. On the other hand, the transmission coefficient in the transverse mode is increased substantially by addition of the SC molecules (see Fig. 5.6). The transverse wave has the maximum displacement 2.25 times as large as that in the case without the SC molecules as seen in Fig. 5.7 (d). In addition, the wave in the right end-region appears to have little phase shift. We therefore conclude that addition of the SC molecules makes the transverse phonons transfer better with faster group velocities in the polymer sub-system. It is in accord with the statement that the bisA molecules in the polymer sub-system are stiffened effectively by addition of the SC molecules. Possible reason of the significant effect of the SC molecules on the transverse wave is that the SC molecules bond vertically to the surface α-alumina and hence work as resistance to the displacement parallel to the surface in the transverse mode.

5.3 Comparison between the simulation results and theoretical predictions

We compare the present results with theoretical predictions with respects to the phonon transmission coefficient (t_{ab}) and the interfacial thermal conductance ($J/\Delta T$). As stated in Chap.1.2. we consider two theoretical models for transmission coefficient: the AMM and the DMM. Continuity of both displacement and stress at the interface gives the AMM transmission coefficient for the phonon with frequency in the common frequency range as

$t_{ab}^{\mathrm{AMM}} = 4Z_a Z_b \mu_a \mu_b / (Z_a \mu_a + Z_b \mu_b)^2$ in Eq. (1.10), In the DMM, the phonons scattered at the interface are assumed to lose fully the information of the incident directions. The $t_{ab}^{\mathrm{DMM}} = v_b g_b(f) / [v_a g_a(f) + v_b g_b(f)]$ in Eq. (1.15) . Setting $v_b/v_a = 0.18$, $Z_b/Z_a = 0.04$, and $\theta_a = \theta_b = 0$ for the present interface (medium-a is the α-alumina, medium-b is the polymers), we find $t_{ab}^{\mathrm{AMM}} = 0.16$. The $t_{ab}^{\mathrm{DMM}} = 0.03$ using the Debye approximation for phonons. The transmission coefficient for the longitudinal acoustic phonon with $\eta = 39.0\,\text{Å}$ in the case of $D = 33.0\,\text{Å}$ without the SC molecules is about 0.09 (see Fig. 5.6), which indicates a tendency to approach the t_{ab}^{AMM} at longer η. Similar observations for the longitudinal acoustic phonons were reported also for other systems as the grain boundary of Si and the interface of the Lennard-Jones solids with different atomic masses, through the wave-packet dynamics simulations [14,59]. As expected, the present transmission coefficients at a short wavelength of $\eta = 13.0\,\text{Å}$ (see Fig. 5.6) compare well with the t_{ab}^{DMM}.

As for the interfacial thermal conductance, the Landauer formula that uses the equilibrium phonon population (P) at the local temperature, has commonly been used: The Landauer formula gives $3.5\,\mathrm{MW/K \cdot m^2}$ for the AMM (Eq. (1.12)) and $12.6\,\mathrm{MW/K \cdot m^2}$ for the DMM (Eq. (1.16)). Those are much smaller than the present values of $100 - 250\,\mathrm{MW/K \cdot m^2}$ in Fig. 4.3 (b). The analytical formulas that take into account non-equilibrium effects in P , predict larger values than the Landauer ones: $3.6\,\mathrm{MW/K \cdot m^2}$ for the AMM (Eq. (1.15)) and $14.0\,\mathrm{MW/K \cdot m^2}$ for the DMM (Eq. (1.17)) . Those values are still much smaller than the present ones. The significant differences indicate importance of atomic scale inhomogeneity and anisotropicity to predict the interfacial thermal conductance of the present model, as well as inappropriateness of the phonon picture in the polymer sub-system.

5.4 Conclusions

In the NEMD, we show that the interfacial thermal conductance is increased by adding the SC molecules. We explain the microscopic mechanisms through combined analyses of atomic vibration spectra of the polymer

sub-system and phonon wave-packet dynamics simulation. The atomic vibration spectra analysis through the equilibrium MD simulation is performed to clarify the changes in the vibrational properties of the polymer sub-system by decreasing its depth and by adding the SC molecules. By performing the phonon wave-packet dynamics simulation we investigate the transmission coefficient through the interface for the wave packet characterized by the wavelength and mode.

We found that three mutually relating reasons through the analyses. First the phonon population of the bisA molecules at those frequencies corresponding to that of acoustic phonons of α-alumina is enhanced by addition of the SC molecules. The bisA molecules become effectively stiffer through entanglement of the bisA and SC molecules. Second the phonon transmission coefficient from the α-alumina slab to the polymer sub-system is increased significantly for the transverse acoustic mode by addition of the SC molecules bonding to surface Al's of α-alumina. The vertical bonding of the SC molecules to the α-alumina surface works as resistance to the displacement parallel to the surface in the transverse mode. Third the group velocities of transverse acoustic mode are increased by addition of the SC molecules due to their roles of the resistance.

In addition we compare the simulation results with theoretical predictions with respects to the phonon transmission coefficient and the interfacial thermal conductance. The two theoretical models are considered the AMM and the DMM. Transmission coefficients with wave packet dynamics at a short wavelength compare well with the DMM. On the other hand, in a long wavelength case indicate a tendency to approach the AMM. As for the interfacial thermal conductance, theoretical predictions are much smaller than the that in NEMD. These results suggested that theoretical predictions for the interface of the polymer-ceramic composite is difficult because the phonon picture is not applicable in polymer sub-system which has atomic scale inhomogeneity and anisotropicity.

Chapter 6

Summary

In this thesis we have studied interfacial thermal conductance between filler and polymer in the heat dissipation material. The mechanisms of the enhanced thermal conductance of the polymer-filler interfaces by adding the surface-coupling agent in the heat dissipation material, that is observed experimentally, are investigated through combined analyses of the non-equilibrium molecular dynamics (NEMD), polymer configurations, atomic vibration spectra of the polymer sub-system and phonon wave-packet dynamics simulation. A simulation system is composed of α-alumina as the filler, bisphenol-A (bisA) epoxy molecules as the polymers, and model molecules for the surface-coupling agent. The inter-atomic potential between the α-alumina and surface-coupling molecule, which is essential in the present simulation, is constructed to reproduce the calculated energies with the electronic density-functional theory. We have adopted the CMAS inter-atomic potential for α-alumina and the Dreiding inter-atomic potentials for the bisA and SC molecules. We consider that the simulation system of polymer-filler interfaces separately by the situation of small and high packing fraction of fillers.

Let us summarize the results obtained from our studies of the interfacial thermal conductance between α-alumina-bisA as follow:

(I) As for the situation of small packing fraction of fillers, we investigate

effects of the surface-coupling molecules on heat transfer by changing their lengths and density. Through the non-equilibrium molecular dynamics, we produce heat flux that directs from the α-alumina to bisA regions by controlling the local temperatures in the bisA and α-alumina regions. We calculate the effective thermal conductivity of the interface area using the heat flux, surface area, and temperature profile in the system. We have found that the thermal resistance at the α-alumina-bisA interface becomes smaller when either larger number of the SC molecules is added at the interface or their lengths are longer. We have found that the effective thermal conductivity of the system approaches to the value estimated by assuming zero thermal resistance at the interface. On the other hand the effective thermal conductivity appears to be saturated for small thermal resistance. In this situation, the contribution of the bisA region to the effective thermal conductivity is dominant.

(II) We consider the heat-transfer routes from the SC molecules to bisA molecules by calculating the atomic temperature (time-averaged kinetic energies) for each atom around the SC molecules in the non-equilibrium run. The heat transfer routes are identified under the assumption that the difference in the atomic temperatures of a pair of atoms gets smaller as the degree of thermal conductance between the two atoms becomes smaller. In the large number and long SC molecules cases, heat is therefore transferred more efficiently between the α-alumina and SC molecule and inside the SC molecule than between the SC and bisA molecules. On the other hand, when the number of the SC molecules is small, heat transfer is more efficient between the SC and bisA molecules than between the α-alumina and SC molecule. In the situation a substantial proportion of heat is transferred from the C of the SC molecule to the O of neighboring bisA molecules.

(III) As for the situation of high packing fraction of fillers, we perform a series of the NEMD runs by changing the polymer depth and adding the

SC molecules to understand their effects on the interfacial thermal conductance. We treat a simulation system where a nanometer-depth polymer sub-system is sandwiched between two α-alumina slabs. The high and low temperature-controlled regions are set in the α-alumina slabs by controlling the local temperature. We find that the interfacial thermal conductance is decreased by decreasing the polymer depth toward the chain length of a single bisA molecule. Through analysis of the polymer configurations, we explain that the reason has resulted from the decrease in the phonon transmission coefficient relating to effectively weakened interaction between a bisA molecule and two α-alumina slabs. The weakening has resulted because the orientation constraint on the bisA molecule due to attachment of each of the two epoxy groups to each of the two α-alumina slabs, lowers the density of the bisA atoms at the interface. However, for smaller polymer-depth cases, deterioration of interfacial thermal conductivity is reduced by adding the SC molecules to the polymer sub-system.

(IV) We have performed combined analyses of the atomic vibration spectra of the polymer sub-system and phonon wave-packet dynamics simulation to explain enhancement mechanisms of the interfacial thermal conductivity of by adding the SC molecules. We have found enhancement of the following three quantities by addition of the SC molecules. First the phonon population of the bisA molecules at those frequencies corresponding to that of acoustic phonons of α-alumina. The bisA molecules become effectively stiffer through entanglement of the bisA and SC molecules. Second the phonon transmission coefficient from the α-alumina slab to the polymer sub-system is increased significantly for the transverse acoustic mode by addition of the SC molecules bonding to surface Al's of α-alumina. The vertical bonding of the SC molecules to the α-alumina surface works as resistance to the displacement parallel to the surface in the transverse mode. Third the group velocities of transverse acoustic mode are increased by addition of the SC molecules due to their roles of the resistance.

(VI) We compare the simulation results with theoretical predictions with respects to the phonon transmission coefficient and the interfacial thermal conductance. The two theoretical models are considered the AMM and the DMM. Transmission coefficients with wave packet dynamics at a short wavelength compare well with the DMM. On the other hand, in a long wavelength case indicate a tendency to approach the AMM. As for the interfacial thermal conductance, theoretical predictions are much smaller than the that in NEMD. These results suggested that theoretical predictions for the interface of the polymer-ceramic composite is difficult because the phonon picture is not applicable in polymer sub-system which has atomic scale inhomogeneity and anisotropicity.

There exist a number of issues that need be improved in future researches: (i) We have used one of the simplest model molecules for the bisA epoxy polymer and surface-coupling agent in the present study. Depending on the application, the bisA epoxy polymers are controlled to polymerize and cross-link with other molecules. (ii) The bond-formation reactions of surface-coupling molecules with filler material are complex combinations of hydrolysis and condensation reactions. We have adopted the ideal situation of bonding between the O in the SC molecule and Al of α-alumina in the present study. (iii) In the phonon wave-packet dynamics simulation, to trace the time-evolution of kinetic and potential energy, the system is cooled down to nearly zero temperature before adding the initial wave-packet with quite small amplitude. In the situation, the phonons experience little anharmonicity of the inter-atomic potential and the polymer configuration differs much from the one at a finite temperature. As for the issues (i) and (ii), the first-principle MD simulation or hybrid quantum-classical simulation, in which reacting atoms are treated with the DFT method, can be used for improvement albeit requiring high computation power. We will challenge to perform the first-principle MD simulation or hybrid quantum-classical simulation to treat compex combination reaction near the polymer interface. Relating to the issue (iii), we can take ensemble of atomic configurations at a finite temperature with the static inverted forces added on all atoms to fix them. The phonon wave-packet dynamics simulation in such systems can be an improvement.

Appendix A

Acoustic mismatch model

The AMM model assumes that continuity of both displacement and stress at the interface gives all phonons reflect secularly with no scattering at the interface. Displacements in a medium a and medium b is written as follows:

$$U_a = A_a \exp\left[i\left(\frac{2\pi f}{v_{a,z}} \cdot z - 2\pi f \cdot t\right)\right] + B_a \exp\left[i\left(\frac{-2\pi f}{v_{a,z}} \cdot z - 2\pi f \cdot t\right)\right], \qquad (a.1)$$

$$U_b = A_b \exp\left[i\left(\frac{2\pi f}{v_{b,z}} \cdot z - 2\pi f \cdot t\right)\right], \qquad (a.2)$$

where A_a, B_a, and A_b are amplitude of waves. As for the first term on the right hand side of Eq. (a.1) is displacement by incident wave, the second term is displacement by reflected wave at the interface. The right hand side of Eq. (a.2) is displacement by transmitted wave. By the two assumptions of continuity of displacement and stress at the interface (z=0), The relations are obtained as follows:

From the assumption of continuity of displacement $U_a = U_b$

$$A_a + B_a = A_b, \qquad (a.3)$$

and the assumption of continuity of stress $F\frac{\partial U_a}{\partial z} = F\frac{\partial U_b}{\partial z}$

$$\frac{2\pi f}{v_{a,z}}FA_a - \frac{2\pi f}{v_{a,z}}FB_a = \frac{2\pi f}{v_{b,z}}FA_b, \qquad (a.4)$$

where F is force at the interface. The relation between F and v as

$$v = \sqrt{F/\rho}\,, \tag{a.5}$$

where ρ is mass density. Using Eq. (a.5) and (a.4),

$$Z_a\,\mu_a A_a - Z_a\,\mu_a B_a = Z_b\,\mu_b A_b\,, \tag{a.6}$$

where $Z_i = \rho_i v_i$, $v_{i,z} = v_i\cos\theta_i$, and $\mu_i = cos\theta_i$.

Comparing Eq. (a.3) and Eq. (a.6), the rate of transmitted amplitude and reflected amplitude to incident amplitude are

$$\frac{B_a}{A_a} = \frac{Z_a\,\mu_a - Z_b\,\mu_b}{Z_a\,\mu_a + Z_b\,\mu_b}\,, \tag{a.7}$$

$$\frac{A_b}{A_a} = \frac{2Z_a\,\mu_a}{Z_a\,\mu_a + Z_b\,\mu_b}\,. \tag{a.8}$$

energy in medium i by wave is expressed as $\frac{1}{2}\rho_i v_i\,\mu_i(2\pi f)^2 A_i^2$. We consider energy balance between medium a and medium b

$$\frac{1}{2}Z_a\,\mu_a(2\pi f)^2 A_a^2 - \frac{1}{2}Z_a\,\mu_a(2\pi f)^2 B_a^2 = \frac{1}{2}Z_b\,\mu_b(2\pi f)^2 A_b^2\,. \tag{a.9}$$

The transmission and reflection coefficient are obtained by dividing Eq. (a.9) by $Z_a\,\mu_a(2\pi f)^2 A_a^2$

$$1 - \frac{Z_a\,\mu_a B_a^2}{Z_a\,\mu_a A_a^2} = \frac{Z_b\,\mu_b A_b^2}{Z_a\,\mu_a A_a^2}\,. \tag{a.10}$$

The reflection coefficient $t_{aa'}$ is

$$t_{aa'} = \frac{Z_a\,\mu_a B_a^2}{Z_a\,\mu_a A_a^2} = \left(\frac{Z_a\,\mu_a - Z_b\,\mu_b}{Z_a\,\mu_a + Z_b\,\mu_b}\right)^2\,. \tag{a.11}$$

The transmission coefficient t_{ab} is

$$t_{ab} = \frac{Z_b\,\mu_b A_b^2}{Z_a\,\mu_a A_a^2} = \frac{4Z_a Z_b\,\mu_a\,\mu_b}{(Z_a\,\mu_a + Z_b\,\mu_b)^2}\,. \tag{a.12}$$

Acknowledgements

Nomenclature

A	parameter for phonon lifetime or parameter for the CAMS potential
B	parameter for the CAMS potential
C	parameter for the CAMS potential
D	depth of polymer sub-system
D_e	energy parameter for the Morse
dt	simulation time step
E	potential energy
F	force vector
f	phonon frequency or parameter for the CAMS potential
G	interfacial thermal conductance
g	phonon density of states
h	Planck' constant
i	imaginary number
J	heat flux per unit area
K_{ij}	parameter for the Dreiding potential
K_{ijk}	parameter for the Dreiding potential
k_B	Boltzmann constant
L	simulation system size
l	z-direction distance
m	mass of atom
N	number of atom
n	number density or index nature number
n_s	number of sampling point
n_{jk}	parameter for the Dreiding potential periodicity
P	phonon population
q	atomic charge parameter for the CAMS potential or Coulomb term
R	averaged displacement
r	position vector of atom
r_{ij}	distance between atoms i and j
r_{ij_eq}	equilibrium distance between atoms i and j
T	temperature

T_{req}	target temperature
t	time
$t_{ab}(t_{ba})$	transmission coefficient from medium a(b) to medium b(a)
V	volume of a material
V_{jk}	parameter for the Dreiding potential
v	phonon group velocity

Greek symbols

ΔT	temperature drop at a interface
ε	energy parameter for the van der Waals
η	wavelength vector
γ	lattice parameter for the Morse potential
Λ	thermal conductivity of a system
λ	thermal conductivity of a material
$\varphi_{ijkl,eq}$	Initial phase shift
ρ	mass density
σ	lattice parameter for the van der Waals or statistical error
τ	phonon lifetime
$\theta_{ijk,eq}$	Equilibrium angle

Subscripts

0	initial
1	high temperature of z-position
2	low temperature of z-position
a	medium a
b	medium b
D	Debye
eq	equilibrium
i, j, k	atom index
l	longitudinal acoustic polarization or atom index
n	number of (CH_2) in a SC molecule

neq non-equilibrium

t   transverse acoustic polarization

group, g group atoms in a molecule

References

[1] S. Mallik, N. Ekere, C. Best, and R. Bhatti, Appl. Thermal Eng. **31**, 355 (2011)

[2] X. C. Tong, Advanced Materials for Thermal Management of Electronic Packaging (Springer, NY, 2011).

[3] R. W. Johnson, J. L. Evans, P. Jacobsen, J. R. Thompson, and M. Christopher, IEEE Trans. Electron. Packag. Manuf. **27**(3), 164 (2004).

[4] D. W. Sundstrom and Y. D. Lee, J. Appl. Polym. Sci. **16**, 3159 (1972).

[5] Z. Shi, M. Radwan, S. Kirihara, Y. Miyamoto, and Z. Jin, Appl. Phys. Lett. **95**, 224104 (2009).

[6] X. Lu and G. Xu, J. Appl. Polym. Sci. **65**, 2733 (1997).

[7] Y. Agari, A. Uneda, and S. Nagai, J. Appl. Polym. Sci. **49**, 1625 (1993).

[8] C. P. Wong and R. S. Bollampally, J. Appl. Polym. Sci. **74**, 3396 (1999).

[9] Y. S. Xu, D. D. L. Chung, and C. Mroz, Composites, Part A **32**, 1749 (2001).

[10] H. Hirano, J. Kadota, T. Yamashita, and Y. Agari, Int. J. Chem. Biol. Eng. **6**, 29 (2012).

[11] P. L. Kapitza, J. Phys. USSR **4**, 181 (1941).

[12] E. T. Swartz and R. O. Pohl, Rev. Mod. Phys. **61**, 605 (1989).

[13] S. Pettersson and G. D. Mahan, Phys. Rev. B **42**, 7386 (1990).

[14] S. Merabia and K. Termentzidis, Phys. Rev. B **86**, 094303 (2012); J. Phys.: Conf. Ser. **395**, 012115 (2012).

[15] I. M. Khalatnikov, Zh. Eksp. Teor. Fiz. **22**, 687 (1952)

[16] W.A. Little, Canadian J. Phys. **37**, 224 (1959)

[17] D. G. Cahill, W. K. Ford, K. E. Goodson, G. D. Mahan, A. Majumdar, H. J. Maris, R. Merlin, and S. R. Philpot, J. Appl. Phys. **93**, 793 (2003).

[18] E. T. Swartz and R. O. Pohl, Appl. Phys. Lett. **51**, 2200 (1987).

[19] A. J. C. Ladd, B. Moran, and W. G. Hoover, Phys. Rev. B **34**, 5058 (1986).

[20] D. P. Sellan, E. S. Landry, J. E. Turney, A. J. H. McGaughey, and C. H. Amon, Phys. Rev. B **81**, 214305 (2010).

[21] G. Casati, in Foundations of Physics, Vol. 16 (Plenum, N. Y., 1986), p. 51.

[22] S. Maruyama and S. H. Choi, Thermal Sci. & Eng. **9**, 1 (2001).

[23] S. Ogata, Y. Hanai, and Y. Shibutani, J. Soc. Mater. Sci. Jpn. **55**, 754 (2006).

[24] G. Kikugawa, T. Ohara, T. Kawaguchi, E. Torigoe, Y. Hagiwara, and Y. Matsumoto, J. Chem. Phys. **130**, 074706 (2009).

[25] K. Sasikumar and P. Keblinski, J. Appl. Phys. **109**, 114307 (2011).

[26] A. R. Abramson, C.-L. Tien, and A. Majumdar, J. Heat Transfer **124**, 963 (2002).

[27] M. Hu, S. Shenogin, and P. Keblinski, Appl. Phys. Lett. **91**, 241910 (2007).

[28] T. Luo and J. R. Llyd, J. Adv. Funct. Mater. **22**, 2495 (2012).

[29] E. S. Landry and A. J. H. McGaughey, Phys. Rev. B **80**, 165304 (2009).

[30] S. Maruyama, Microscale Thermophys. Eng. **7**, 41(2003).

[31] J. Shiomi, and S. Maruyama, Phys. Rev. B **73**, 205420 (2006).

[32] P. K. Schelling, S. R. Phillpot, and P. Keblinski, Appl. Phys. Lett. **80**, 2484 (2002).

[33] P. K. Schelling, S. R. Phillpot, and P. Keblinski, J. Appl. Phys. **95**, 6082 (2004).

[34] Z. T. Tian, B. White, and Y. sun, Appl. Phys. Lett. **96**, 26113(2010).

[35] N. A. Roberts and D. G. Walker, J. Appl. Phys. **108**, 123515(2010).

[36] R. Landauer, Philos. Mag, **21**, 863 (1970).

[37] S. Simons, J. Phys. C **7**, 4048 (1974).

[38] M. P. Allen and D. J. Tildesley, *Computer Simulation of Liquids* (Clarendon, Oxford, 1987).

[39] S. R. White, P. T. Mather, and M. J. Smith, Polym. Eng. Sci. **42**, 53, (2002).

[40] J. F. Fu, L. Y. Shi, Q. D. Zhong, Y. Chen, and L-Y, Chen, Polym. Adv. Tecnol. **22**, 1032 (2010).

[41] J. P. Pascault and R. J. J. Williams, *Epoxy polymer* (Wiley, NJ, 2010).

[42] C. Li, G. A. Medvedev, E-W. Lee, J. Kim, J. M. Caruthers, and A. Strachan, Polymer **53,** 4222 (2012).

[43] B. Arab and A. Shokuhfar, J. Nano-Electronic Phys. **5**, 01013 (2013).

[44] M. Matsui, Phys. Chem. Minerals **23**, 345 (1996).

[45] S. L. Mayo, B. D. Olafson, and W. A. Goddard III, J. Phys. Chem. **94**, 8897 (1990).

[46] J. Gasteiger and M. Marsili, Tetrahedron **36**, 3219 (1980).

[47] B. Delley, J. Chem. Phys. **92**, 508 (1990).

[48] B. Delley, J. Chem. Phys. **113**, 7756 (2000).

[49] J. P. Perdew, K. Burke, and M. Ernzerhof, Phys. Rev. Lett. **77**, 3865 (1996).

[50] CRC *Handbook of Chemistry and Physics*, 67th., edied by R. C. Weast (CRC Press, Boca Raton, FL, 1983).

[51] J. B. Wachtman, Jr., W. E. Tefft, D. G. Lam, and R. P.Stinchfield, J. Res. Natl. Bur. Stand. **64A**, 213 (1960); J. B. Wachtman, Jr., in *Mechanical and Thermal Properties of Ceramics*, editrd by J. B. Wachtman, Jr. (NBS, Washington, 1969), p. 139.

[52] K. C. Hass, W. F. Schneider, A. Curioni, and W. Andreoni, Science **282**, 9, 265 (1998).

[53] I. Frank, D. Marx, and M. Parrinello, J. Chem.Phys. **104**, 8143 (1996).

[54] I. Manassidis, A. DeVita, and M. J. Gllian, Surf. Sci. Lett. **285**, 517 (1993).

[55] K. Tanaka, S. Ogata, R. Kobayashi, T. Tamura, M. kitsunezuka, and A. Shinma, J. Appl. Phys. **114**, 193512 (2013).

[56] I. C. Yeh and M. L. Berkowitz, J. Chem. Phys. **117,** 3155, (1999).

[57] B. Li, L. Wang, and G. Casati, Phys. Rev. Lett. **93**, 184301 (2004).

[58] M. Hu, P. Keblinski, and B. Li, Appl. Phys. Lett. **92,** 211908 (2008).

[59] S.Aubry, C. J. Kimmer, A. Skye, and P. K. Schelling, Phys. Rev. B **78**,

064112 (2008).

[60] S. Ogata, N. Ohba, and T. Kouno, J. Phys. Chem. C. **117**, 17960 (2013).

[61] S. Ogata, Phys. Rev. B **72**, 045348 (2005).

[62] S. Ogata, Y. Abe, N. Ohba, R. Kobayashi, J. Appl. Phys. **108**, 064313 (2010).